Astron. Astrophys. 338, 223–242 (1998)

ASTRONOMY
AND
ASTROPHYSICS

Millimetre study of star formation in southern globules⋆

Th. Henning[1] **and R. Launhardt**[1,2]

[1] Astrophysikalisches Institut und Universitäts-Sternwarte Jena (AIU), Schillergäßchen 2, D-07745 Jena, Germany (henning@astro.uni-jena.de)
[2] Max-Planck-Institut für Radioastronomie, Auf dem Hügel 69, D-53121 Bonn, Germany (rlau@mpifr-bonn.mpg.de)

Received 28 May 1997 / Accepted 7 July 1998

Abstract. The paper presents the results of a dedicated millimetre continuum and molecular line (CO and CS) search for cold and dense (protostellar) cores and molecular outflows in 35 southern Bok globules (Dec. $\leq -30°$). Only globules which are associated with cold $IRAS$ point sources (FIR colour temperatures below 35 K) were selected for this study.

We could demonstrate that globules are often loosely associated with molecular cloud complexes from which they probably formed. Based on such associations, we determined reliable distances for most of the globules of our sample. It turned out that half of the selected globules are located in the local spiral arm at distances between 170 and 400 pc. The most prominent features in the spatial distribution of these globules are the Lindblad ring and the Vela-Gum complex. A group of 14 globules is located at larger distances (0.7 – 4 kpc) in the Carina arm. The objects in the far Carina arm ($d > 2$ kpc) are clearly different from "classical" Bok globules being more massive and more luminous.

Out of the 35 globules observed, all globules were detected in the ^{12}CO(2–1) line (detection rate 100%, 3 σ detection limit $T_{\rm mb}$ = 0.3 K), 24 globules were detected in the CS(2–1) line (69%, detection limit 0.2 K), and 18 globules were detected in the 1.3 mm continuum emission (51%, detection limit 40 mJy/beam). In 12 globules (34%), CO line wings indicating the presence of molecular outflows have been found, of which 8 outflows were previously unkown. The colours of the embedded $IRAS$ point sources, the strength of the millimetre dust continuum emission, the CS line temperatures as well as the presence of molecular outflows are all well correlated with each other. Based on these results and on the $IRAS$ colour-colour diagram, we can clearly distinguish two groups of sources: Objects with active protostellar cores ("Class 0" and "I") and globules with less dense and less centrally peaked cores (pre-protostellar cores and globules which may not form stars at all).

The objects with active protostellar cores are characterized by centrally condensed cores (typical beam-averaged density of $\approx 10^6 {\rm cm}^{-3}$) and molecular outflows. The mass spectrum ${\rm d}N/{\rm d}M$ of the circum-protostellar envelopes can be fitted with a single slope of -1.8 between 0.15 and 2 $M_\odot$ and a mean mass of 0.6 $M_\odot$. Two objects in our sample clearly resemble the properties of "Class 0" protostars while the majority of the star-forming cores probably already passed the main accretion phase. Five of the colder and less-condensed objects are proposed to be pre-protostellar cores.

Key words: circumstellar matter – stars: formation – ISM: clouds – dust, extinction – ISM: jets and outflows – radio continuum: ISM

1. Introduction

The study of star formation in giant molecular clouds and large dark clouds is complicated by their complex structure. Relatively isolated and compact globules come closer to the theoreticians' view of a dense and isolated cloud core undergoing spherical collapse motion. Recent studies of northern Bok globules clearly demonstrated that they are active sites of low-mass star formation (e.g. Reipurth 1983; Neckel et al. 1985; Clemens & Barvainis 1988 - hereafter C&B88; Clemens et al. 1991 - hereafter CYH91; Yun & Clemens 1992; Zhou et al. 1993; Launhardt & Henning 1997 - hereafter Paper I; Bourke et al. 1997). Many globule cores are associated with very cold far-infrared sources with colour temperatures between 20 and 40 K (C&B88, Persi et al. 1990; Bourke et al. 1995a - hereafter BHR).

In a systematic survey of 59 northern globules for their 1.3 mm dust continuum emission, we detected 21 cold condensations (Paper I). A clear correlation between the mm continuum flux densities, the infrared (IR) spectral indices, and the presence of molecular outflows was found. In general, globule cores with mm continuum emission have spectral energy distributions (SEDs) typical of dense molecular cloud cores with deeply embedded young stellar objects (YSOs) ("self-embedded" protostars). Therefore, it was not surprising that most of the outflow sources were detected at 1.3 mm continuum. In contrast to this, objects with SEDs typical of pre-main sequence (PMS) stars were in general not detected. It was shown that 5 – 7% of all globules contain protostellar cores and that the majority of the globules forms stars with a typical mass of 0.5 $M_\odot$ at some time of their evolution.

Send offprint requests to: R. Launhardt

⋆ Based on observations collected at the European Southern Observatory, La Silla, Chile

Nearly all of the previous investigations were based on the globule catalogue of Clemens & Barvainis (C&B88) which is restricted to declinations north of $-30°$. A gold-mine for a systematic study of globules in the southern sky is the catalogue of 1100 dark clouds and globules compiled from the ESO/SERC J survey plates by Hartley et al. (1986). BHR presented recently a comprehensive list of small isolated Bok globules from this survey including optical and $IRAS$ properties. For these globules, Bourke et al. (1995b) searched for emission in the (1,1) and (2,2) inversion transitions of ammonia. Half of the globules were detected, but only 6% of the sources turned out to be strong ($T_{\rm A}^{*} \leq 0.35$ K). Persi et al. (1990) surveyed 482 small southern dark clouds selected from the Hartley catalogue for evidence of YSOs and found 6% of the clouds to be associated with $IRAS$ point sources with colour temperatures typical of YSOs and PMS stars.

In this paper we present the results of the first systematic search for mm dust continuum emission and molecular outflows from 35 southern globules with cold $IRAS$ sources. The goal of this study was to identify globules with ongoing star formation and to derive their physical properties, such as mass, luminosity, outflow activity, and evolutionary stage. In Sect. 2, we describe the selection criteria for our target list and determine the individual distances towards the globules. The observations and data reduction are described in Sect. 3. In Sect. 4, the results are presented and physical parameters are derived from the data. In Sect. 5, we discuss the properties and the evolutionary stage of the globule cores. The main results are summarized in Sect. 6.

2. The source list

2.1. Target selection

The globules for the mm continuum and line study were selected from the catalogues of Hartley et al. (1986) and Feitzinger & Stüwe (1984) according to the following selection criteria:

1. Isolated location and compact appearance (angular diameter mostly less than $6'$, corresponding to a linear diameter of 0.5 pc at a distance of 300 pc) and
2. Association with cold *IRAS* point sources with $2\,{\rm S}_\nu(25) < {\rm S}_\nu(60) < 0.5\,{\rm S}_\nu(100)$ (${\rm S}_\nu$ are the *IRAS* flux densities at the corresponding wavelengths in μm).

Here, association means that the *IRAS* position is located within the optically visible (opaque) boundaries of the globule. Although it was not a strong selection criterion, most of the selected globules have high extinction values (optically thick in the centre; opacity class A in the nomenclature of Hartley et al. or class 5 or 6GAMMA in the nomenclature of Feitzinger & Stüwe).

In total, we selected 35 globules for our mm continuum and line study. Of these, 15 globules are also contained in the infrared study of Persi et al. (1990) and 20 globules are contained in the list of BHR. Table 1 lists the selected globules together with the names and coordinates of the associated $IRAS$ point sources. For the dark cloud (DC) names, we use the nomenclature of Hartley et al. (1986).

In order to simplify the understanding of the target selection and the interpretation of the data, we subdivided the globules into sub-groups according to the IR broad-band SEDs of the associated *IRAS* point sources, following the classification scheme of Paper I. Here, we use the IR spectral index $\alpha_\nu(\lambda_1 - \lambda_2) = d\log(\nu S_\nu)/d\log(\nu)$. According to the definition of α_ν, the colour temperature increases with increasing spectral indices. One has to keep in mind, however, that the FIR colour temperatures may systematically overestimate the true effective dust temperature of the dense cores if very small, transiently heated grains contribute to the 60 μm emission. Fig. 1 shows the selected sources in the *IRAS* colour-colour diagram. The sample breaks up into the following two groups:

Group 1: Sources which were at least detected at 60 and 100 μm and which have $\alpha_\nu(60-100) \geq -2.3$ and $\alpha_\nu(12-25) < 1$ (20 globules). Their SEDs are steadily rising from 12 to 100 μm, but are much broader than that of a single-temperature blackbody. The FIR spectral index range of this group translates into (colour-corrected) colour temperatures between 23 and 33 K with a mean vaue of 26 K (assuming a dust emissivity going with $\lambda^{-1.5\ldots-2}$). The location of these sources in the colour-colour diagram (Fig. 1) compares well to the location of other star-forming molecular cloud cores (Emerson 1987) and *IRAS* outflow sources (Morgan & Bally 1991). Therefore, they are good candidates for internally heated star-forming cloud cores ("self-embedded" protostars).

Group 2: Sources which were at least detected at 100 μm and which have $\alpha_\nu(60-100) < -2.3$ if they were also detected at 60 μm (12 globules). Their SEDs are steeply rising from 60 to 100 μm. The FIR spectral index range of this group translates into colour temperatures of $16 \ldots 23$ K. With one exception (DC 292.9+1.3), none of these sources was detected at 12 μm. These objects are clearly the coldest objects in our sample. Their FIR fluxes are lower than those of the group 1 sources and are often close to the detection limit of $IRAS$.

The group membership and the $IRAS$ point source flux densities are listed in Table 3. Three globules could not be classified within this scheme. They are marked by "?" in Table 3. Fig. 2 shows the averaged broad-band SEDs of the two groups compiled from the *IRAS* point source fluxes. Here, we excluded the far Carina sources ($d \geq 2$ kpc, see Sect. 2.2) from the averaging procedure.

In contrast to our list of northern globules (Paper I), this sample does not contain any group 3 sources (SEDs which are falling from 12 to 25 μm, candidates for T Tauri stars) nor "star-less" globules (group 4). The selected sample is obviously biased towards globules with deeply embedded YSOs, and therefore is not representative of Bok globules in general nor of the entire star-forming phase.

There are four objects in our sample which were already studied in more detail by other authors. The *IRAS* source 08242−5050 in the globule DC 267.4−7.5 is associated with the spectacular HH jet HH 46−47 and a bipolar molecular out-

Table 1. Coordinates and distances of the selected globules

DC No.	*IRAS* Name	RA(1950) (h m s)	Dec(1950) (° ′ ″)	Other names[a)]	d (pc)	Association[b)], Method[c)]	Ref.[d)]	Rel. class[e)]
249.4−5.1	07435−3430	07 43 34.0	−34 30 38		400	I	1, 2, 3, 11	A
253.3−1.6	08076−3556	08 07 40.2	−35 56 07	BHR12, (i)	400	I	1, 2, 3, 11	A
268.2−9.7	08150−5247	08 15 05.9	−52 47 35		400	I	1, 2, 3, 11	A
265.7−7.7	08171−4933	08 17 11.1	−49 33 47	BHR31	400	I	1, 2, 3, 11	A
267.4−7.5	08242−5050	08 24 16.5	−50 50 44	BHR36, Sa111, (ii)	400	I	1, 2, 3, 11	A
267.2−7.2	08250−5030	08 25 03.4	−50 30 34	BHR34, Sa110	400	I	1, 2, 3, 11	A
267.7−7.4	08261−5100	08 26 11.5	−51 00 39	BHR41, Sa110	400	I	1, 2, 3, 11	A
276.2−10.6	08433−5945	08 43 22.6	−59 45 06	BHR56	400	Ia	1, 2, 3, 11	A
275.9+1.9	09449−5052	09 44 57.0	−50 52 06	BHR55, Sa121	300	Ia, a	2, 4, 11	A
283.8−3.4	10059−5948	10 05 54.4	−59 48 30		3700	IIa, BBW287	5, 6, 13	B
289.3−2.8	10471−6206	10 47 07.1	−62 06 22	BHR58	250	a	4	A
289.9−3.2	10497−6242	10 49 44.8	−62 42 06		3400	IIb, BBW323	5, 6, 13	B
287.1+2.4	10501−5630	10 50 11.2	−56 30 37		3100	IIb, BBW324	5, 6, 13	B
293.3+0.1	11277−6057	11 27 46.6	−60 57 51	BHR63	1300	(IIb), c	6	C
292.9+1.3	11278−5940	11 27 50.0	−59 40 50		4400	IIb, BBW358	5, 6, 13	B
294.3−2.0	11306−6311	11 30 37.9	−63 11 24		2200	IIb, BBW362	5, 6, 13	B
294.9+0.1	11403−6126	11 40 23.9	−61 26 47	BHR67	1300	IIb, BBW372	5, 6, 13	B
296.2−3.6	11431−6516	11 43 10.2	−65 16 19		3600	IIb, BBW371	5, 6, 13	B
295.0+1.3	11436−6017	11 43 36.4	−60 17 23		1300	IIb, BBW372	5, 6, 13	B
295.7+0.0	11488−6045	11 48 49.6	−60 45 49		1300	IIb, BBW372	5, 6, 13	B
297.7−2.8	11590−6452	11 59 03.1	−64 52 11	BHR71, Sa136	200	III	7, 12	A
303.8−14.2	13036−7644	13 03 41.4	−76 44 03	BHR86, Sa160	200	IV	8, 11	A
307.3+2.9	13224−5928	13 22 26.0	−59 28 07	BHR87	1000	IIb, c	5, 6	B
313.3−0.3A	14183−6050	14 18 19.9	−60 50 37		800	(IIb), c	6	C
313.3−0.3B	14188−6054	14 18 49.0	−60 54 39		800	(IIb), c	6	C
313.3−0.3C	14189−6115	14 18 55.7	−61 15 01		800	(IIb), c	6	C
323.0+4.0	15075−5307	15 07 33.2	−53 07 34	BHR106	200	b		C
320.5−3.6	15215−6056	15 21 32.2	−60 56 19	BHR100	170	V	9, 11	A
320.1−4.3	15223−6146	15 22 21.6	−61 46 04	BHR98	170	V	9, 11	A
319.9−4.8	15230−6211	15 23 00.4	−62 11 52	BHR97	170	V	9, 11	A
325.1−1.9	15431−5652	15 43 07.0	−56 52 52		800	(IIb), c	6	C
344.5+3.2	16458−3939	16 45 49.7	−39 39 36		700	(IIb), c	6	C
337.1−4.9	16549−5030	16 54 59.6	−50 30 58		100	VI	10	A
354.0+3.5	17135−3200	17 13 30.8	−32 00 53		200	VII		B
354.2+3.2	17151−3202	17 15 08.6	−32 02 24	BHR167	200	a	4	A
344.6−4.3	17181−4405	17 18 09.3	−44 05 48	BHR137	700	a, (IIb)	4, 6	A
356.5−4.5	17518−3414	17 51 54.0	−34 14 03	BHR168	200	b		C

a) Other names: BHR refers to Bourke et al. (1995a); Sa refers to Sandqvist & Lindroos (1976) and Sandqvist (1977); (i) HH120, CG30-IRS4; (ii) HH46-47

b) Associations: BBW numbers refer to the list of Brand et al. 1986; (I) Gum nebula and Vela Sheet; (Ia) proximity to Gum nebula; (IIa) tangent region of the Carina arm; (IIb) near side of the Carina arm; (III) proximity to Coalsack; (IV) Chamaeleon II dark cloud; (V) proximity to G 317.4–4.0; (VI) associated with HD 152824; (VII) near DC 354.2+3.2

c) Methods: (a) stellar reddening; (b) very few foreground stars, average distance of the local globules in this direction (see text); (c) many foreground stars

d) References: (1) Brandt 1971; (2) Hawarden & Brand 1976; (3) Zealey et al. 1983; (4) Bourke et al. 1995b; (5) Brand & Wouterloot 1988 and Brand & Blitz 1993 (photometric distances); (6) Grabelsky et al. 1987; (7) Seidensticker & Schmidt-Kaler 1989; (8) Whittet et al. 1991; (9) Neckel & Klahre 1980; (10) Westin 1985; (11) Dame et al. 1987; (12) Bourke et al. 1997; (13) Brand et al. 1986.

e) Reliability class: A = highest, C = lowest (see text).

flow (Schwartz 1977; Dopita et al. 1982; Chernin & Masson 1991; Olberg et al. 1992). The cometary globule DC 253.3−1.6 contains the infrared object *IRAS* 08076-3556 which has a steep SED and is located very close to the Herbig-Haro object HH 120 (Persi et al. 1994). NIR images (H_2) show evidence for two outflows in this globule oriented almost perpendicular to each

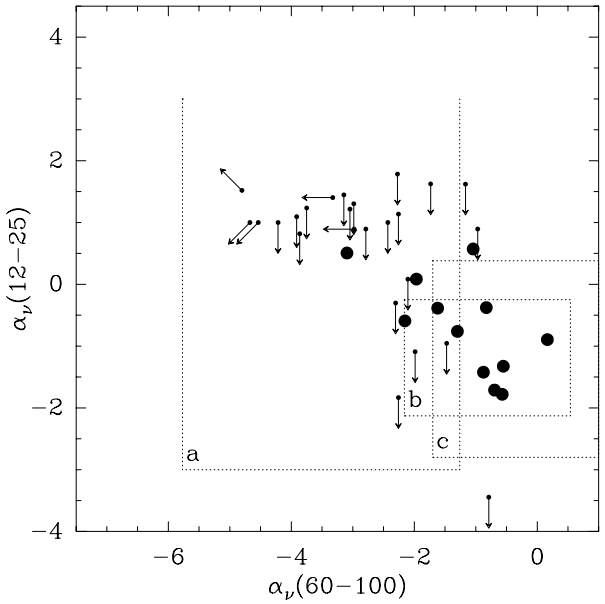

Fig. 1. $IRAS$ colour-colour diagram for all $IRAS$ point sources located in the selected globules. Sources with valid fluxes in all four $IRAS$ bands are marked by large filled circles. Sources which have upper flux limits in one or more $IRAS$ bands are indicated by arrows showing the direction of their possible shift in the diagram. For the sake of comparison, the areas of different object classes are marked in the colour-colour plane by rectangular boxes: (a) Cirrus clouds (Meurs & Harmon 1988), (b) dense molecular cloud cores (Emerson 1987), (c) $IRAS$ outflow sources (Morgan & Bally 1991; Wouterloot et al. 1989).

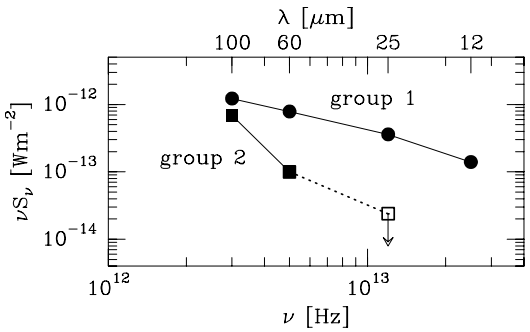

Fig. 2. Averaged IR spectral energy distributions for group 1 (circles) and group 2 (squares) sources. Only globules with $d \leq 1.3$ kpc were considered.

other (Hodapp & Ladd 1995). The sources in DC 253.3−1.6 and DC 267.4−7.5 were already measured at 1.3 mm continuum by Reipurth et al. (1993). The globule DC 297.7−2.8 (BHR 71) which has a deeply embedded YSO driving a collimated bipolar outflow was recently studied in detail by Bourke et al. (1997). The *IRAS* source embedded in the globule DC 303.8−14.2 was found to drive a bipolar molecular outflow and to show spectroscopic evidence for gravitational collapse (Lehtinen 1997).

2.2. Distances

For most of the globules of our list the distances were not known. Therefore, we checked the association of the globules with molecular cloud complexes with well-known distances using the method described in Paper I. Distinct groups of globules are associated, e.g., with the Vela-Gum complex (Zealey et al. 1983) or with molecular clouds in the Carina arm of the Galaxy (Grabelsky et al. 1987). The distances derived in this way are listed in Table 1 together with the associated molecular cloud structures. For some of the selected globules, we adopted the distances derived by BHR from stellar reddening which are consistent with the distances derived by our method.

Following Paper I, we assigned three reliability classes to the derived distances with A being the most reliable distances and C the most uncertain ones. Class B was assigned to most of the globules which are associated with molecular clouds in the Carina arm (photometric distances, Brand & Wouterloot 1988). Four of the class C globules which are located at galactic latitudes between 293° and 345° and which have many foreground stars were associated with the inner edge of the Carina arm. Two other C globules at galactic latitudes of 323° and 356° which have only very few foreground stars were assigned to the average distance of 200 pc of the local globules in this direction.

Figs. 3 and 4 show the galactic distribution of all globules of our sample together with the boundaries of selected molecular cloud complexes. The distance distribution (Fig. 5) has two dominant peaks at 200 and 400 pc which are related to Lindblad's expanding ring of early-type stars and dark clouds ("Gould's Belt"; e.g., Lindblad et al. 1973; Sandqvist & Lindroos 1976) and to the Vela-Gum complex. All globules of this sample which are further away than 500 pc are related to the Carina arm.

The objects in the Carina arm are more distant (> 0.7 kpc) in accordance with the fact that they have more foreground stars than the nearby globules in the local spiral arm. Since we are looking into the relatively empty inter-arm region towards the Carina arm at galactic longitudes between $\approx 285°$ and 360° (see Fig. 3), also relatively distant globules can be seen in this direction. While the most distant objects at longitudes between 285° and 295° (2.2 – 4.4 kpc) are difficult to identify as globules because of their diffuse appearance, the appearance of the more nearby Carina globules at longitudes between 295° and 360° (0.7 – 1.3 kpc) is not very different from that of the local globules. In other directions, the higher stellar density within the local spiral arm prevents the identification of such distant globules from optical surveys.

The average distance of the local globules (excluding all Carina sources) is 300 pc. This value is somewhat smaller than the average distance of 500 pc which we derived for the northern globule sample (Paper I). This discrepancy can be understood if one considers that the Sun is located at the inner ("southern") edge of the local spiral arm. Excluding only the "far" Carina sources ($d > 2$ kpc), the average distance of the selected globules ($d \leq 1.3$ kpc) amounts again to 500 pc.

Table 2. Observational parameters

Line	Frequency $\nu_{\rm o}$ (GHz)	Detector	Beamwidth $\theta_{\rm b}$ ($''$)	Efficiency $\eta_{\rm mb}$	Resolution Δv (km s^{-1})	Reference position offset
continuum	236	bolometer	23			$70''$
^{12}CO(J=2→1)	230	SIS	23	0.60	0.10	$\approx 1^\circ$
CS(J=2→1)	98	Schottky	45	0.70	0.24	$11'$

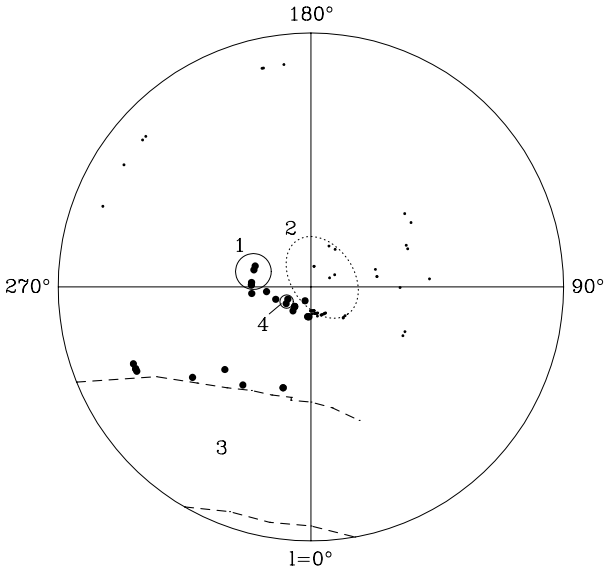

Fig. 3. Galactic (longitude–distance) distribution of the observed globules within a radius of 1.7 kpc around the Sun. The globules are marked by large dots. The globules of the northern sample (Paper I) are shown as small dots for the sake of comparison. Some selected molecular cloud complexes are marked by open circles or ellipses: (1) Gum nebula, (2) Lindblad Ring - Gould's Belt, (3) Carina arm, (4) Chamaeleon II and Coalsack. Note that there are more Carina sources between l=285° and 300° at larger distances (2.2 – 4.4 kpc).

3. Observations and data reduction

The 1.3 mm continuum and molecular line observations at 1.3 and 3 mm were performed at the 15-m SEST telescope at La Silla, during March 1995 (ESO N° 54.C-0343). All objects listed in Table 1 were observed in the mm continuum as well as in the ^{12}CO(2–1) and CS (2−1) lines. The observing parameters are summarized in Table 2.

3.1. Millimetre continuum observations

For the 1.3 mm continuum observations, we used the ^{3}He-cooled SEST facility bolometer system (Kreysa 1990). The effective beam size at this wavelength is $23''$ (HPBW). We followed the standard chopping beam-switching ON-ON observing procedure. The positions observed are the $IRAS$ point source positions listed in Table 1. Chopping was provided by a focal plane chopper operating at 6 Hz with a beam separation of $70''$ in azimuth. Beam-switching was done by nodding the telescope after 10 sec of integration by $70''$ in azimuth and thus shifting the object from one beam into the other. One measurement was formed by 10 ON-ON pairs with a total integration time of 200 s. The number of measurements spent on one object depended on the achieved signal-to-noise ratio.

The atmospheric transmission was measured by skydips every two hours. Pointing was done by doing cross scans on a nearby bright quasar. The telescope pointing was found to be repeatable within $\pm 5''$. Mars was used as primary flux density calibrator. We estimate the total calibration uncertainty to be ≈ 20 %. The average $3\,\sigma$ detection limit of the entire survey is 40 mJy/$23''$beam.

The raw data were de-spiked, averaged for each ON-ON pair, and corrected for the atmospheric extinction using the approximation of a plane-parallel atmosphere. The mean value of all measurements towards one position was averaged by using weighting factors of σ_i^{-2} where σ_i are the standard deviations for each ON-ON pair.

3.2. CO and CS molecular line observations

The CO(J=2→1) observations at 230 GHz were performed with a SIS receiver. For the 3 mm band (CS(J=2→1) at 98 GHz), the telescope was equipped with a Schottky mixer receiver. The system temperatures during the observations were in the range 450 – 550 K at 230 GHz and 400 – 460 K at 98 GHz. As backend, an Acousto Optical Spectrometer with a total bandwidth of 86 MHz and 2000 channels was used. The beam sizes, main beam efficiencies, and velocity resolutions are listed in Table 2.

The CO observations were done in the position switching mode with OFF positions 1 to 1.5° away from the ON positions. The reference positions were checked for CO emission by frequency switching observations. The CS observations were performed in the dual beam switching mode with a beam throw of $11'$ in azimuth. Pointing was regularly checked with nearby bright SiO sources.

The standard chopper wheel method (Penzias & Burrus 1973; Kutner & Ulich 1981) was used for intensity calibration, resulting in the antenna temperature $T_{\rm A}^*$ which is corrected for atmospheric attenuation and telescope losses. To get the main beam brightness temperature, $T_{\rm mb}$, $T_{\rm A}^*$ was divided by the main beam efficiency $\eta_{\rm mb}$. Typical $1\,\sigma$ rms values for the CO and CS spectra are 0.11 K and 0.07 K ($T_{\rm mb}$), respectively. Data reduction was done with the CLASS software.

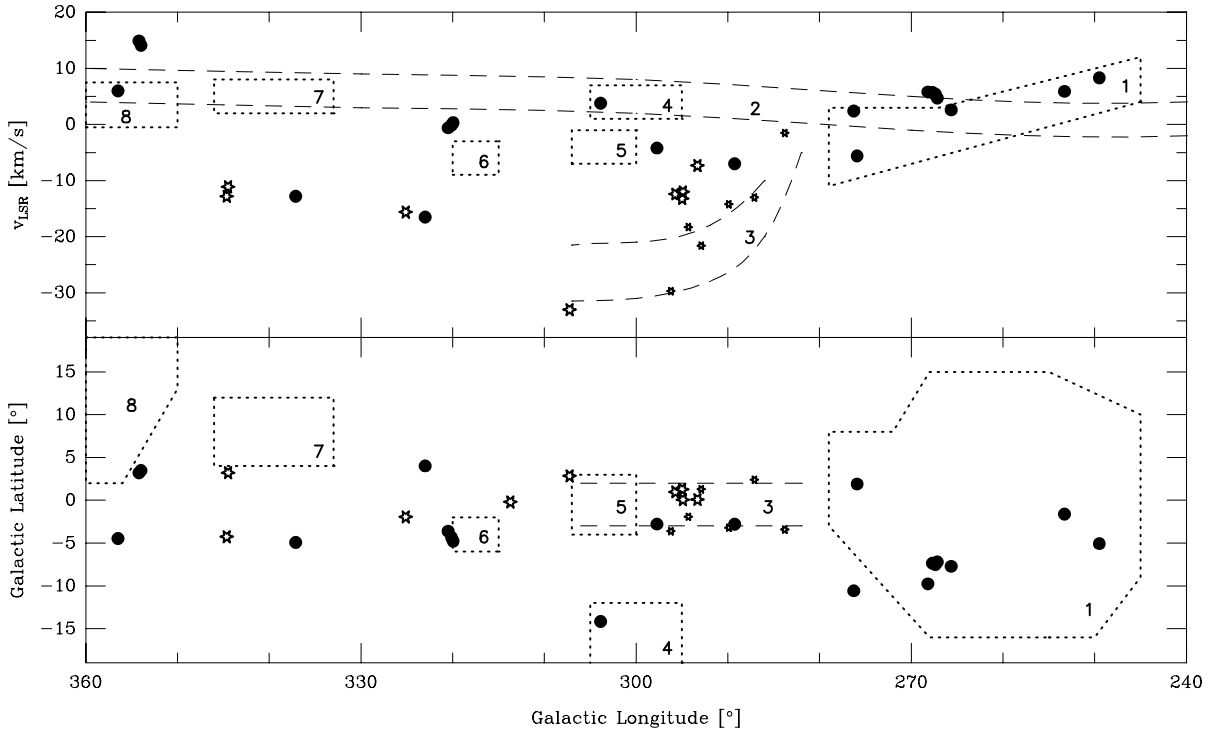

Fig. 4. Galactic distribution of the observed globules. Lower panel: Longitude-latitude diagram. Upper panel: Longitude-velocity diagram. Local globules which are located within 400 pc from the Sun are marked by filled circles. Globules which are associated with the "near" (700 – 1300 pc) and "far" Carina arm (>2 kpc) are indicated by large and small asterisks, respectively. Some selected molecular cloud complexes are marked by dotted boxes and dashed lines: (1) Gum nebula and Vela Sheet (400 pc), (2) Lindblad Ring - Gould's Belt ($\approx 160-300$ pc; indicated by dashed lines), (3) Carina arm (indicated by dashed lines), (4) Chamaeleon II (200 pc), (5) Coalsack (175 pc), (6) G 317.4−4.0 (170 pc), (7) Lupus dark cloud (170 pc), (8) Ophiuchus dark cloud complex (160 pc).

4. Results and derived properties

4.1. General survey statistics

Out of the 35 globules observed, all globules were detected in the ^{12}CO(2–1) line ($3\,\sigma$ detection limit $T_{\rm mb} = 0.3$ K), 24 globules were detected in the CS(2–1) line (detection rate 69%, detection limit 0.2 K), and 18 globules were detected in the 1.3 mm continuum emission (51%, detection limit 40 mJy/beam). Due to the differences in nature and distances of the sources, we analyse the results separately for the following object groups: local goup 1 sources ($d < 500$ pc, $\langle d \rangle = 300$ pc; 9 objects), local group 2 sources (9 objects), sources in the near Carina arm (0.7 kpc $< d <$ 1.3 kpc, $\langle d \rangle = 0.9$ kpc; 10 objects), and sources in the far Carina arm (2.2 kpc $< d <$ 3.7 kpc, $\langle d \rangle = 3.2$ kpc; 6 objects). The objects in the Carina arm belong mostly to group 1. Three objects could not be classified and one globule (DC 313.3−0.3) contains three $IRAS$ sources (all group 1).

The ASURV[1] software package was used for the statistical analysis of the results. This package performs a "survival analysis" which takes upper limits into account. Parameter distributions and mean values were derived by the cumulative Kaplan-Meier estimator. Two-sample tests were performed in order to check the significance of differences or similarities in the parameter distributions of the globule groups.

4.2. Millimetre continuum data

4.2.1. Detection statistics

In Table 3, we compile the measured 1.3 mm continuum flux densities per beam together with the r.m.s. noise and the $IRAS$ point source fluxes (detected objects are printed boldface). For non-detections, the $3\,\sigma$ detection limits are listed. Five of the detected sources were meanwhile mapped with the bolometer at 1.3 mm. The maps were already or will be discussed in more detail in other papers (Bourke et al. 1997; Launhardt et al. 1998b).

The overall detection rate of 51% for the 1.3 mm continuum radiation in this survey is higher than the rate of 35% obtained for the northern globule sample (Paper I). The reason for this discrepancy is that due to our selection criteria the southern sample investigated here is much more biased towards globules with embedded protostars than the northern sample (cf. Sect. 2.1). Excluding the far Carina sources in the southern sample and counting only group 1 and 2 sources in the northern sample, the overall detection rate of the southern sample amounts to 50% vs. 70% for the northern sample. The reason for the lower detection rate in this southern survey compared to the northern survey is probably the lower sensitivity of the SEST observations ($3\,\sigma$

[1] ASURV Rev. 1.2 (LaValley, Isobe & Feigelson 1992) is a software package which implements the methods presented in Feigelson & Nelson (1985).

Table 3. Results – *IRAS* and 1.3 mm fluxes, luminosities, and masses

DC No.	*IRAS* Name	Group	S_{12} [Jy]	S_{25} [Jy]	S_{60} [Jy]	S_{100} [Jy]	$S_{1.3\mathrm{mm}}$ [mJy/Ω_b]	L_bol [$\mathrm{L}_\odot$]	$L_{1.3\mathrm{mm}}$ [$\mathrm{L}_\odot/\Omega_\mathrm{b}$]	M_gas [$\mathrm{M}_\odot/\Omega_\mathrm{b}$]	Rem.[a]
249.4−5.1	07435−3430	2	<0.25	0.18	2.40	19.94	**25± 8**	2.8E+0*	6.2E−5	1.1E−1	
253.3−1.6	08076−3556	1	0.63	3.73	18.25	47.54	**552±23**	1.7E+1	1.4E−3	2.3E+0	M
268.2−9.7	08150−5247	2	<0.34	0.29	2.85	22.51	<48	3.6E+0*	<1.2E−4	<2.0E−1	
265.7−7.7	08171−4933	2	<0.25	<0.25	<0.72	13.06	<24	–	<6.0E−5	<1.0E−1	
267.4−7.5	08242−5050	1	0.82	6.31	26.13	58.27	**256±15**	1.7E+1*	6.3E−4	1.1E+0	M
267.2−7.2	08250−5030	2	<0.25	<0.25	1.19	17.08	<51	2.4E+0*	<1.3E−4	<2.2E−1	
267.7−7.4	08261−5100	1	0.91	2.50	4.29	10.91	**38±11**	6.8E+0	9.4E−5	1.6E−1	
276.2−10.6	08433−5945	1	<0.32	0.18	1.83	9.74	<54	2.2E+0*	<1.3E−4	<2.3E−1	
275.9+1.9	09449−5052	1	<0.25	<0.27	8.16	22.30	**104±16**	2.9E+0*	1.5E−4	2.5E−1	
283.8−3.4	10059−5948	1	<0.25	0.65	4.26	23.03	**84± 8**	3.9E+2*	1.8E−2	3.0E+1	f.C.
289.3−2.8	10471−6206	2	<0.25	0.27	5.36	37.11	**57±14**	2.1E+0*	5.5E−5	9.4E−2	M
289.9−3.2	10497−6242	1	<0.25	2.00	15.48	81.73	**120±15**	9.5E+2*	2.2E−2	3.7E+1	f.C.
287.1+2.4	10501−5630	1	<0.25	1.16	7.73	35.53	**145±11**	4.7E+2	2.2E−2	3.7E+1	f.C., M
293.3+0.1	11277−6057	2	<0.77	<0.88	1.08	12.95	<42	2.2E+1*	<1.1E−3	<1.9E+0	n.C.
292.9+1.3	11278−5940	2	1.19	1.71	4.51	36.53	<45	1.0E+3	<1.4E−2	<2.3E+1	f.C.
294.3−2.0	11306−6311	1	2.31	12.74	104.80	231.60	**39± 9**	1.4E+3*	2.9E−3	5.0E+0	f.C.
294.9+0.1	11403−6126	2	<0.60	0.56	3.57	43.91	<42	5.9E+1*	<1.1E−3	<1.9E+0	n.C.
296.2−3.6	11431−6516	1	11.85	47.62	388.80	595.50	**109±12**	1.3E+4	2.2E−2	3.7E+1	f.C.
295.0+1.3	11436−6017	1	0.32	1.03	3.86	19.32	**65±14**	6.8E+1	1.7E−3	2.9E+0	n.C.
295.7+0.0	11488−6045	?	0.39	0.29	<2.49	22.69	<30	3.1E+1*	<7.9E−4	<1.3E+0	n.C.
297.7−2.8	11590−6452	1	<0.25	6.53	77.38	192.90	**1257±17**	1.0E+1*	7.8E−4	1.3E+0	M
303.8−14.2	13036−7644	1	<0.25	1.05	6.38	22.57	**274±16**	1.7E+0*	1.7E−4	2.9E−1	
307.3+2.9	13224−5928	1	1.20	2.35	8.18	37.21	**125±17**	5.7E+1*	1.9E−3	3.3E+0	n.C.
313.3−0.3A	14183−6050	1	5.58	20.34	239.10	773.60	**60±10**	5.0E+2	6.0E−4	1.0E+0	n.C.
313.3−0.3B	14188−6054	1	2.09	15.29	284.10	675.20	**212±11**	5.0E+2	2.1E−3	3.6E+0	n.C.
313.3−0.3C	14189−6115	1	1.80	4.98	75.54	287.90	<36	1.7E+2*	<3.6E−4	<6.1E−1	n.C.
323.0+4.0	15075−5307	2	<0.25	<0.25	<0.67	11.34	<36	–	<2.2E−5	<3.8E−2	
320.5−3.6	15215−6056	1	<0.25	0.49	3.39	16.55	**43±11**	6.0E−1	1.9E−5	4.0E−2	
320.1−4.3	15223−6146	2	<0.25	<0.25	2.01	11.59	<39	3.8E−1*	<1.7E−5	<3.0E−2	
319.9−4.8	15230−6211	2	<0.25	0.20	2.01	15.38	<51	4.9E−1*	<2.3E−5	<3.9E−2	
325.1−1.9	15431−5652	1	<1.12	0.71	8.79	26.59	<48	2.9E+1	<4.8E−4	<8.1E−1	n.C.
344.5+3.2	16510−4026	1	<0.84	<0.76	6.68	35.27	<48	1.7E+1	<3.6E−4	<6.2E−1	n.C.
337.1−4.9	16549−5030	?	0.41	<0.28	<0.63	12.21	<48	–	<7.4E−6	<2.0E−2	
354.0+3.5	17135−3200	?	0.86	0.93	<3.39	25.87	<39	1.1E+0*	<2.4E−5	<5.0E−2	
354.2+3.2	17151−3202	1	<1.66	1.05	10.81	43.68	<48	2.2E+0	<3.0E−5	<5.0E−2	
344.6−4.3	17181−4405	1	2.65	3.63	59.88	170.00	**90±16**	9.7E+1*	6.8E−4	1.2E+0	n.C.
356.5−4.5	17518−3414	2	<0.44	<0.37	1.40	15.85	<54	6.7E−1*	<3.4E−5	<5.8E−2	

a) Remarks: M = 1.3 mm bolometer map will be published in a succeeding paper; n.C. = near Carina source ($d \leq 1.3$ kpc); f.C. = far Carina source ($d > 2$ kpc).

∗ No NIR photometry available. The given luminosities are obtained by integrating the flux densities between 7 and 1300 μm.

detection limit of 40 mJy/beam) compared to the IRAM observations of the northern globules (17 mJy/beam).

Since the uncertainty of the *IRAS* positions (major axis of the position error ellipse) is often as large as the SEST beam at 1.3 mm (13″ to 36″ with a mean of 23″±7″ vs. a beam size of 23″), the measured mm fluxes probably do not always correspond to the emission maximum. This could especially apply to the group 2 sources which were not detected in the shorter *IRAS* bands. On the other hand, we do not expect the group 2 sources to have point-like mm emission, so that the detection rates should not be biased (cf. Sect. 5.5).

Despite of this uncertainty, the detection rates for the two globule groups differ significantly from each other, viz. 77% vs. 17% for group 1 and 2, respectively. For the local sources, the detection rates are 78% (gr. 1) and 22% (gr. 2). These detection rates compare well to rates obtained for the northern sample (Paper I; 94% for group 1, 20% for group 2). Although the far Carina sources have much higher masses and luminosities than the local globules and are, therefore, assumed to be of different nature (cf. Sects. 4.2 and 5.2), we found no significant difference in the detection rates between the local and the Carina sources.

4.2.2. Masses and column densities

Table 3 also lists the total gas mass per beam for the sources detected at 1.3 mm. The masses were derived from the 1.3 mm continuum flux densities by assuming optically thin configurations and an isothermal, uniformly distributed population of dust grains (see Paper I). To avoid confusion, we applied a uniform set of parameters for the derivation of mass to all objects: a dust opacity of 0.8 cm^2 per gram of dust (Ossenkopf & Henning 1994), a total gas-to-dust mass ratio of 150 (see Paper I), and an average dust temperature of 25 K. The dust temperature was derived from greybody fits to the sub-mm/mm SEDs of ten northern globule cores with similar *IRAS* characteristics (Launhardt et al. 1997; nine sources were group 1, one source group 2) and is consistent with the FIR colour temperature of these objects (cf. Sect. 2.1).

All masses were derived under the assumption of optically thin dust emission which certainly holds for most objects since massive disks (optically thick at 1.3 mm) were shown to be rare (Terebey et al. 1993). The assumption that the mm continuum emission arises mainly from optically thin circumstellar envelopes than from optically thick disks is supported by the correlation between S_ν(1.3 mm) and T(CS) (Fig. 6) since disks emit comparatively little line emission. The relative uncertainty of the derived masses is estimated to be a factor of 2, due to the imprecisely known values of the mass opacity κ_m and the dust temperature (see Henning et al. 1995, or Gordon 1995 for a discussion of the uncertainties in masses derived from submillimetre continuum data). To approximately correct the derived masses for the actual dust temperature, the mass has to be scaled with $\approx T_\mathrm{d}$(adopted)/T_d. This also means that the derived masses are not very sensitive to the adopted temperature.

With the above input parameters, we derive masses of 0.04 to 2.3 $\mathrm{M}_\odot$/beam for the local group 1 sources ($d \leq 500$ pc), with a mean value of 0.6$\pm$0.25 $\mathrm{M}_\odot$/beam. The average mass of the local group 2 sources is 0.05$\pm$0.01 $\mathrm{M}_\odot$/beam, with the only two detected objects having masses of $\approx$ 0.1 $\mathrm{M}_\odot$/beam. Adopting a more realistic dust temperature of 20 K and a lower dust opacity value of 0.5 $\mathrm{cm}^2\,\mathrm{g}^{-1}$ for the group 2 sources, the derived masses would increase by a factor of two. The average 3 σ detection limit for the local sources is 0.2 $\mathrm{M}_\odot$/beam. The masses of the Carina sources (mainly group 1) range from 1 to 37 $\mathrm{M}_\odot$/beam with average values of 1.7$\pm$0.4 $\mathrm{M}_\odot$/beam and 29$\pm$6 $\mathrm{M}_\odot$/beam for the near and far Carina sources, respectively. The mean beam-averaged column densities of the (local) group 1 and 2 sources are $\langle N_\mathrm{H}\rangle_{\mathrm{gr.1}}$ = (5$\pm$5) $10^{22}\mathrm{cm}^{-2}$ and $\langle N_\mathrm{H}\rangle_{\mathrm{gr.2}}$ = (1$\pm$0.5) 10^{22} cm^{-2}, respectively. The significance of the difference in the detection rates and masses between the two groups will be discussed in more detail in Sect. 5.2.1.

At a distance of 300 pc, the HPBW of 23″ corresponds to a linear diameter of 0.033 pc or $\approx$ 7000 AU, respectively, which is smaller than the diameter of an infalling protostellar envelope at an infall age of some 10^5 yrs (sound speed of 0.2 $\mathrm{km\,s}^{-1}$, see Sect. 5.4). For the local sources, the measured continuum fluxes can, therefore, be assigned to "circumstellar" material. Since the sources may be more extended than the beam, the derived masses are, however, lower limits to the total circumstellar masses. The masses derived for the more distant (Carina) sources may include more extended material which is probably not "circumstellar".

The circumstellar masses can also be derived from the 100 μm *IRAS* fluxes. Here, we use the same effective dust temperature of 25 K and a dust opacity of 80 cm^2 per gram of dust (Ossenkopf & Henning 1994). The assumption of optically thin emission holds at this wavelength for all sources when assuming that the bulk of the emission does not originate from a compact disk. We find a good correlation (r = 0.91) between the masses derived from the 1.3 mm continuum emission and from the 100 μm *IRAS* point source fluxes, although the two mass estimates are not exactly equal, but differ systematically. While the mm masses of the local group 1 sources are, on average, 2.5 times higher than the 100 μm masses, the mm masses of the (detected) local group 2 sources are only half as large as the 100 μm masses. The systematically lower $M_\mathrm{env}^{1.3\mathrm{mm}}/M_\mathrm{env}^{100\mu\mathrm{m}}$ ratio of the group 2 sources compared to the group 1 sources suggests that these objects are more extended than the group 1 sources. Obviously, the derived mm masses per beam underestimate the total masses of the group 2 sources stronger than those of the group 1 sources. In general, the relative good agreement between the 1.3 mm masses (HPBW = 23″) and the 100 μm *IRAS* masses suggests that the bulk of the dust continuum emission from these sources arises from a core which is more compact than 23″. This applies estecially to the group 1 sources. There is no evidence that the bulk of the dust in these sources is too cold to be detected by *IRAS* at 100μm.

4.2.3. Densities

At the current stage of investigation we have no information about the morphology and the total masses of the globule cores. However, the higher mm flux densities (and masses) per beam and the stronger CS lines (cf. Sect. 4.3.4) suggest that the group 1 sources are more centrally condensed than the group 2 sources and have, thus, higher central densities. Considering only the local globules ($d \leq 500$ pc), the beam-averaged volume densities (derived from the continuum emission under the assumption of spherical sources with diameters corresponding to the beam size) of the group 1 sources range from 5 10^4 to 5 10^6 cm^{-3}, with a mean value of $(8 \pm 5)\,10^5$ cm^{-3}. In case of an internal density gradient, which we expect to be present in such star-forming cores, the local densities in the core centres may be much higher.

In contrast, the group 2 sources have a mean beam-averaged volume density of $\leq (0.6 \pm 0.3)\,10^5$ cm^{-3}, with the two sources detected at 1.3 mm continuum (DC 249.4$-$5.1 and 289.3$-$2.8) having a mean density of 1 10^5 cm^{-3}. In spite of the larger beam size, these densities compare well to the values derived for the northern globule sample (Paper I). The critical density of the CS (2$-$1) line is 3 10^5 cm^{-3} which is just between the mean beam-averaged densities of the two object groups. Hence, the densities derived from the dust continuum emission are consistent with the finding that group 1 globules have in general CS

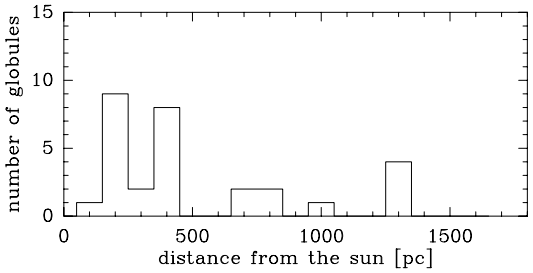

Fig. 5. Distance distribution of the observed globules. The width of the bins is 100 pc. Note, that the far Carina sources are beyond the distance limit of the diagram.

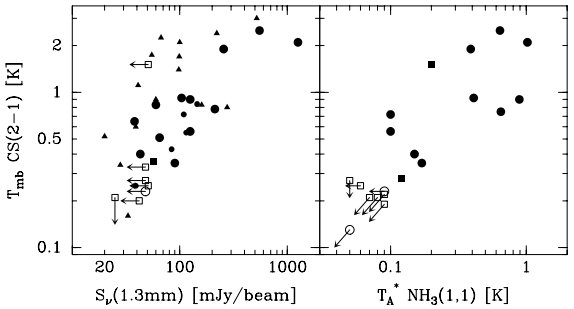

Fig. 6. CS(2–1) line peak temperature ($T_{\rm mb}$) vs. 1.3 mm flux density (left panel) and NH_3 line peak temperature ($T_{\rm A}^*$) (Bourke et al. 1995b, right panel) for all globule cores which were detected in at least one of the two tracers. Group 1 sources are marked by large circles and group 2 sources by squares. Far Carina sources (d > 2 kpc, all group 1) are indicated by small circles (only in right panel). Empty symbols and arrows indicate upper limits. For the sake of comparison, the northern group 1 sources (Paper I, smaller HPBW!) are shown as triangles in the right diagram.

cores while group 2 globules mostly don't have CS cores (cf. Sect. 4.3.1). The beam-averaged densities of the Carina sources are by more than an order of magnitude lower than those of the local globules which results from the large projected beam size.

4.2.4. Luminosities

Table 3 also lists the bolometric luminosities $L_{\rm bol}$ and the 1.3 mm luminosities $L_{1.3{\rm mm}}$. The 1.3 mm luminosity $L_{1.3{\rm mm}}$ was calculated with a bandwidth of $\delta\nu$ = 50 GHz. The bolometric luminosities were obtained by integrating under the NIR fluxes taken from Persi et al. (1990), the $IRAS$ point source fluxes, and the 1.3 mm fluxes. If a source was not detected in the lower $IRAS$ bands, a value of one half of the upper limit was adopted for the last non-detected band. The flux densities of all other non-detected bands were set to zero. For the wavelength region from 135 to 1300 μm, we integrated under grey-body curves fitted to the 60, 100, and 1300 μm fluxes. If no NIR photometry was available for a source, we list the luminosity integrated between 7 and 1300 μm. The luminosity of these young objects comes mainly from the FIR spectral region where the SEDs have their maximum (between 100 and 300 μm). Note, however, that for group 1 sources the NIR contribution to $L_{\rm bol}$ can be as high as 30% (e.g., DC 267.7−7.4). For the group 2 sources which are assumed not to have embedded YSOs and of which none was found to have an optical counterpart (star or nebulosity), the contribution from wavelengths shorter than 7 μm is negligible.

The local objects span a luminosity range between 0.3 and 17 $L_\odot$, with the mean values of the group 1 and 2 sources being 6.7±2.0 $L_\odot$ and 1.5±0.4 $L_\odot$, respectively. The average luminosities of the near and far Carina sources are 50±15 $L_\odot$ (without DC 313.3−0.3) and 800±400 $L_\odot$ (without DC 296.2−3.6), respectively. The far Carina source DC 296.2−3.6 has an exceptional high luminosity ($1.3\,10^4$ $L_\odot$). There are no significant differences between group 1 and 2 sources in the Carina arm.

One has to keep in mind that more than one object may contribute to the *IRAS* luminosity due to the large beam of *IRAS*. This could especially apply to the more distant objects. The derived luminosity may also be different from the bolometric luminosity if the source is not spherically symmetric (see, e.g., Men'shchikov & Henning 1997). The assumption of spherical symmetry (isotropic emission) is, however, assumed to be fulfilled for deeply embedded sources without optical or NIR counterparts. In spite of these uncertainties, there is the general tendency that group 1 objects are more luminous than group 2 objects and that objects with higher luminosities are associated with more massive globule cores (cf. Fig. 11).

4.3. Molecular line data

4.3.1. Detection statistics

The results of the CO and CS line observations are summarized in Table 4. We list the centre velocity $v_{\rm LSR}$, the main beam temperature $T_{\rm mb}$, the line width Δv (FWHM), and the integrated line intensity $\int T_{\rm mb} dv$ for both lines. The given temperatures are the observed peak line temperatures corrected for the main beam efficiency. The line widths and center velocities were obtained from Gaussian fits to the lines after masking out line wings, self absorption features, and line components at other but nearby velocities. The integrated line intensities include the emission from line wings. If a line was contaminated by a second component (e.g. DC 275.9+1.9), this second line was modeled with a Gaussian profile and subtracted before integrating under the line of interest.

All sources were detected in the CO line. If more than one CO line was detected, the CS emission was used to discriminate between the globule and foreground or background CO emission. The detection rates for the CS (2−1) line emission are similar to those for the dust continuum emission. While the overall detection rate in the CS line is 69% (detection limit $T_{\rm mb}$ = 0.2 K), the detection rates for the (local) group 1 and 2 sources are 90% and 40%, respectively. As for the mm continuum emission, we found no significant difference in the CS detection rates between the local and the Carina sources. Fig. 6 (left panel) shows that there is a clear correlation between the mm continuum flux densities and the CS line peak temperatures. The objects which were not detected in one of the two tracers are

Table 4. Results – CO and CS line parameters

DC No.[a]	Group	^{12}CO (J = 2 → 1):						CS (J = 2 → 1):				
		$v_{\rm LSR}$ [km s^{-1}]	$T_{\rm mb}$ [K]	Δv [km s^{-1}]	$\int T_{\rm mb} dv$ [K km s^{-1}]	$F_{\rm CO}$ [b]	Rem. [c]	$v_{\rm LSR}$ [km s^{-1}]	$T_{\rm mb}$ [K]	Δv [km s^{-1}]	$\int T_{\rm mb} dv$ [K km s^{-1}]	Rem. [c]
249.4−5.1	2	8.3	1.9	1.5	3.0		l2(46 km/s)	–	<0.21	–	–	
253.3−1.6	1	6.0	6.6	2.4	26.5	7.3E-5	**w2**, ws	6.2	2.50	1.2	2.60	wr
268.2−9.7	2	5.8	6.5	1.6	11.2		l2(1.5 km/s)	6.0	0.33	0.7	0.24	
265.7−7.7	2	2.6	5.5	1.1	6.4			–	<0.27	–	–	
267.4−7.5	1	5.4	8.2	1.7	24.0	3.0E-5	**w2**, ws	5.3	1.90	0.9	2.00	wr
267.2−7.2	2	4.7	6.8	1.5	11.1			4.8	1.51	0.9	1.56	
267.7−7.4	1	5.7	5.5	2.4	15.5	2.4E-6	**wb**, ww	5.6	0.65	0.9	0.58	
276.2−10.6	1	2.4	2.0	1.3	2.6			–	<0.13	–	–	
275.9+1.9	1	−5.5	2.6	3.3	12.9	1.3E-5	**w2**, l2(−0.6 km/s)	−5.3	0.92	1.0	1.00	
283.8−3.4*	1	−1.5	5.8	3.3	24.5	1.0E-4	**w2**	−0.8	0.43	1.6	0.70	
289.3−2.8	2	−7.0	6.5	2.5	17.6		lss	−7.2	0.28	1.5	0.55	lsa
289.9−3.2*	1	−14.2	7.2	2.8	22.5	7.4E-5	**wr**, ww	−14.2	0.55	1.5	0.84	
287.1+2.4*	1	−13.0	7.6	4.2	35.6	1.5E-4	**w2**, ww	−13.2	1.00	1.6	1.16	wb
293.3+0.1	2	−7.3	2.1	1.8	4.1			–	<0.21	–	–	
292.9+1.3*	2	−21.6	3.9	2.7	11.0			–	<0.11	–	–	
294.3−2.0*	1	−18.3	8.0	4.0	42.9		lss	−18.0	0.25	2.5	0.54	
294.9+0.1	2	−12.0	6.0	1.4	9.2			−11.8	0.20	1.0	0.19	
296.2−3.6*	1	−30.4	13.5	2.5	36.6		lsa, l2(−27.9 km/s)	−30.3	0.72	1.6	1.23	
295.0+1.3	1	−13.2	5.4	2.3	16.6	1.1E-4	**w2**	−13.2	0.51	1.2	0.66	
295.7+0.0	?	−12.4	5.2	1.5	8.5			−12.5	0.40	0.9	0.38	
297.7−2.8	1	−4.1	8.9	3.2	50.0	2.0E-4	**w2**, ws, lsa	−4.4	2.10	1.3	3.30	w2
303.8−14.2	1	3.7	8.5	3.3	32.7	8.1E-6	**w2**, lsa	3.7	0.90	2.0	2.10	wb
307.3+2.9	1	−33.0	6.7	2.3	17.1			−32.9	0.56	1.1	0.68	
313.3−0.3A	1	−42.5	9.6	2.7	36.5		ll	−42.7	0.83	1.9	1.67	
313.3−0.3B	1	−42.3	5.4	4.9	–		lsa, ll	−42.5	0.78	2.4	1.45	
313.3−0.3C	1	−38.6	5.4	3.8	17.7		ll	–	<0.20	–	–	
323.0+4.0	2	−16.5	2.7	1.6	4.6			–	<0.19	–	–	
320.5−3.6	1	−0.6	4.6	1.4	6.9			−0.4	0.40	1.5	0.67	
320.1−4.3	2	−0.1	4.8	1.4	6.9			–	<0.22	–	–	
319.9−4.8	2	0.3	7.3	1.8	14.7			0.6	0.25	2.1	0.45	
325.1−1.9	1	−15.6	1.9	1.8	3.8			–	<0.21	–	–	
344.5+3.2	1	−11.1	4.1	1.5	6.5			–	<0.21	–	–	
337.1−4.9	?	−12.8	2.7	1.8	5.4			−12.6	0.27	0.9	0.27	
354.0+3.5	?	14.1	5.2	1.4	7.5			–	<0.21	–	–	
354.2+3.2	1	14.9	6.1	1.8	12.5			15.0	0.23	1.5	0.37	
344.6−4.3	1	−12.8	9.5	2.5	35.0	2.5E-5	**wb**, lss	−12.9	0.35	1.5	0.56	
356.5−4.5	2	6.0	2.1	1.6	4.3	2.4E-7	**wr**, ww	–	<0.21	–	–	

$*$ far Carina source ($d > 2$ kpc)

a) DC names of sources with CO line wings (outflow candidates) are printed boldface

b) Outflow momentum flux $F_{\rm CO}$ in units of [M$_\odot$ km s^{-1} yr^{-1}] (see Sect. 5.3)

c) Remarks: w2 = 2 wings; wr = red wing; wb = blue wing; ww = weak wing; ws = strong wing; l2 = second line at given $v_{\rm LSR}$; lsa = line shows self-absorption dip; lss = line is strongly saturated; ll = several lines

mostly close to the detection limit in the other tracer. For the sake of comparison, we included the northern globule sources (only group 1, Paper I) in the diagram. The northern sources tend to have stronger CS lines compared to the southern sources. Note, however, that the IRAM observations of the northern globules were performed with a smaller beam than the SEST observations of the southern globules. The higher beam filling factor of the dense gas in the smaller beam might explain the stronger CS lines of the northern sources. Although no distance effects nor the different beam sizes of the continuum and CS observations were considered here, this correlation indicates that the optically thin CS line keeps growing with column density (cf. discussion in Launhardt et al. 1998a; see also Paper I).

We also evaluated the ammonia survey of Bourke et al. (1995b). Out of the 20 globules of our sample which were observed in NH_3 by these authors, 12 globules belong to group 1

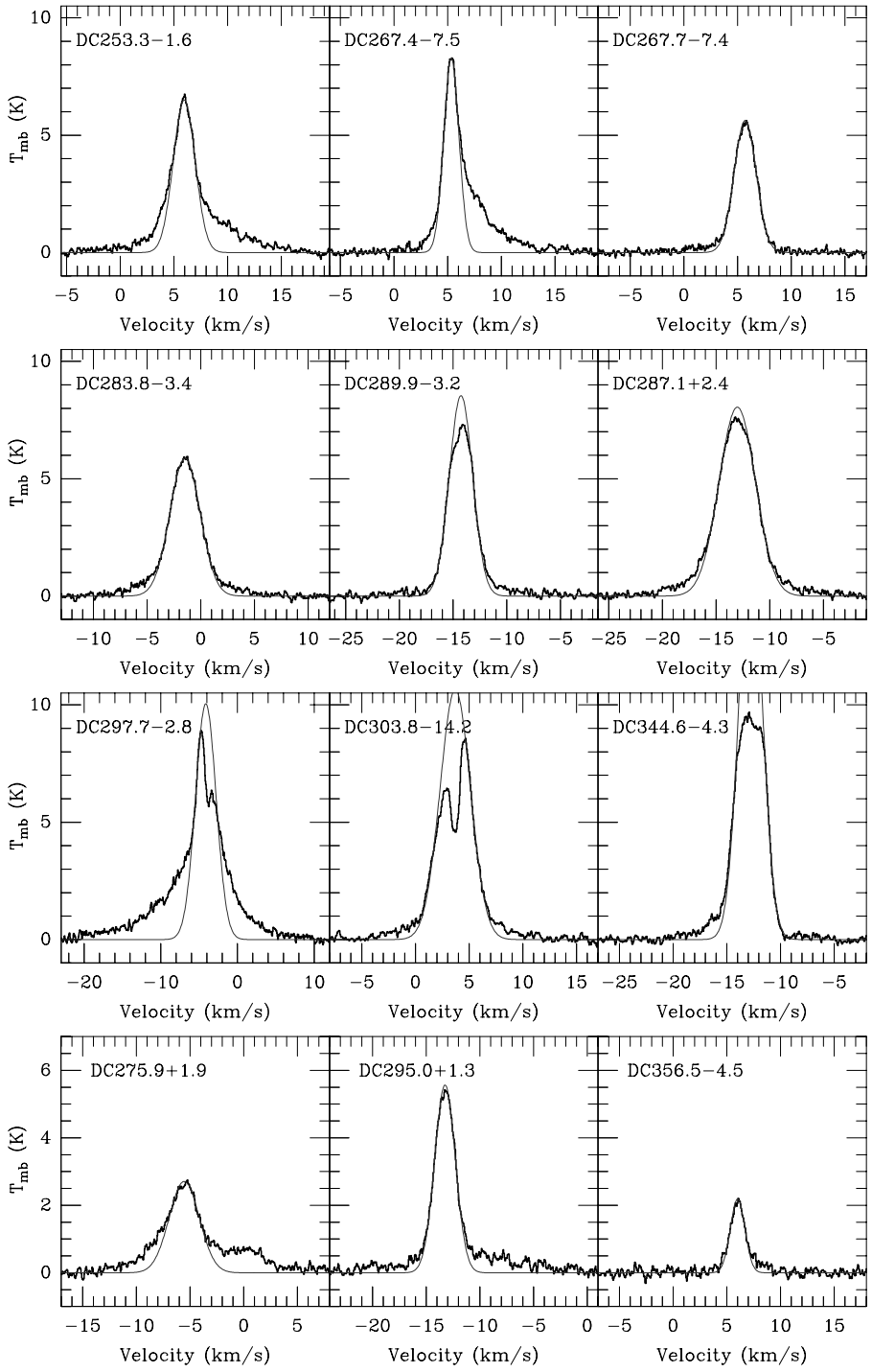

Fig. 7. ^{12}CO J=2–1 spectra (taken at the positions given in Table 1) of the 12 sources showing line wings. The thin lines are Gaussian fits to the CO lines (see text).

and 8 globules to group 2. The NH_3 detection rates for the two globule groups are very similar to those for the CS line or for the mm continuum, viz. 83% for group 1 and 37% for group 2. Fig. 6 (right panel) shows the clear correlation between the peak temperatures of both lines. It can also be seen that group 1 sources have, on average, much stronger lines than group 2 sources. The only exceptions from this rule are DC 267.2−7.2 - a local group 2 source with strong lines (cf. Sect. 5.1), and DC 276.2−10.6 and 354.2+3.2 - two local group 1 sources with very weak lines. All three objects were not detected at 1.3 mm continuum.

Alltogether, these results show that the 1.3 mm dust continuum, CS, and NH_3 are all roughly equivalent tracers of dense, star-forming globule cores.

4.3.2. CO(2–1) line characteristics

The ^{12}CO (2−1) line temperatures ($T_{\rm mb}$) of the local globules range from 1.9 K (DC 275.9+1.9) to 8.9 K (DC 297.7−2.8),

with mean values 5.9±0.8 K and 5.3±0.6 K for group 1 and 2 sources, respectively. Assuming that the CO line is optically thick and thermalized, the mean radiation temperatures translate into kinetic gas temperatures of 11 K and 10 K for group 1 and 2 sources, respectively. These values compare well to the mean kinetic temperature derived for the northern globules (≈ 10 K; CB88; CYH91; Lemme et al. 1996; see also Paper I). For six of the southern group 1 globules, Bourke et al. (1995b) derived an average kinetic gas temperature of $\langle T_{\rm kin} \rangle \approx 13$ K (from NH_3, HPBW = 1′.4).

The peak line temperatures of the two globule groups differ only marginally, indicating high optical depths and similar kinetic gas temperatures. The linewidths and, hence, the integrated intensities differ more significantly. Here, we consider only the Gaussian cores of the lines but not the line wings. The mean linewidth and integrated intensity for group 1 (local objects) are 2.3±0.25 km s^{-1} and 20.4±4.6 K km s^{-1} vs. 1.6±0.13 km s^{-1} and 9.4±1.7 K km s^{-1} for group 2. Although the line broadening can have many reasons (e.g., turbulence, outflows, infall, rotation) which do not necessarily have something to do with star-formation activity, the broader CO lines of the group 1 sources indicate that these globules have a more complex gas dynamics than the group 2 globules. The average CO linewidths compare well to the linewidths found for the northern globules (CYH91; see Paper I).

No significant difference in the CO line parameters was found between the local globules and the near Carina sources. However, the far Carina sources ($d \leq 2$ kpc, mostly group 1) have higher CO line temperatures (8.4±1.2 K), broader lines (3.4±0.3 km s^{-1}), and larger integrated intensities (32±3.5 K km s^{-1}) than the local globules. Taking into account a lower beam filling factor for these distant sources, their mean kinetic gas temperature must be higher than 15 K (see discussion in Sect. 5.6).

4.3.3. Outflows

In 12 globules CO line wings were found indicating the presence of molecular outflows (DC numbers printed boldface in Table 4). Five of the objects with CO line wings have also wings in the CS line (also marked in Table 4). The CO(2–1) spectra of the 12 outflow candidates are shown in Fig. 7. All spectra were taken towards the positions listed in Table 1. In addition, these objects are marked in the colour-colour diagram (Fig. 8). It can be clearly seen that most of the sources with strong millimetre continuum emission show outflow activity and vice versa (cf. Cabrit & André 1991; Bontemps et al. 1996).

Of the 12 sources showing line wings, four objects were already known to have outflows: DC 253.3−1.6, 267.4−7.5, 297.7−2.8, and 303.8−14.2 (for references see Sect. 2.1). All four objects are local group 1 sources. The first three of these objects are those with the strongest line wings in our sample. These three sources have also high mm continuum fluxes corresponding to high circumstellar masses ($M_{\rm env} = 1.1 \ldots 2.3\,{\rm M}_\odot$, see Table 3) indicating that they are very young (cf. discussion in Sect. 5.4). In case of 8 globules, we detected CO line wings for the first time, which increases the known number of globules with outflows considerably. This shows that the outflow phenomenon is quite widespread in this kind of globules and ultimatively proofs that we see evidence for star formation in these objects.

Out of the 12 outflow candidates 11 objects belong to the group 1 and one object (DC 356.5−4.5) belongs to group 2. Excluding again all Carina arm sources, 6 out of 9 group 1 globules and one out of 9 group 2 globules have outflows. This gives an outflow rate of 67% for group 1 which is nearly the same value as the rate of 65% derived for the northern group 1 globules (Yun & Clemens 1992; Paper I). All group 1 outflow sources were also detected at 1.3 mm continuum. DC 356.5−4.5 (group 2) is the only source with a CO line wing which was not detected at 1.3 mm continuum nor in the CS line. Since the detected (red) line wing is very weak, we cannot exclude that this line wing is caused by an independent velocity component and has possibly nothing to do with an outflow. Very weak line wings were further found in the CO spectra of DC 267.7−7.4 (local globule, gr. 1) and 289.9−3.2 (far Carina arm).

Eight of the 11 outflow candidates remaining (excluding DC 356.5−4.5) were found to have both blue and red line wings indicating the presence of bipolar outflows. The red wing in the spectrum of DC 275.9+1.9 is probably blended by a second line. Two globules (DC 267.7−7.4, and 344.6−4.3) have only blue line wings and one globule (DC 289.9−3.2) has only a red line wing. Summarizing these results, we find that most of the detected outflows are bipolar and that neither blue nor red monopolar outflows are dominating the sample. Typical outflow velocities (maximum velocity extent from the line center at the 0.2 K $\sim 2\,\sigma$ level) are ≈ 7 km s^{-1} ($3 \ldots 17$ km s^{-1}).

4.3.4. CS(2–1) line characteristics

The CS (2−1) peak line temperatures ($T_{\rm mb}$) of the detected sources vary between 0.2 K (DC 294.9+0.1) and 2.5 K (DC 253.3−1.6) with a mean value of 0.7±0.2 K, a mean linewidth of 1.3±0.1 km s^{-1}, and a mean integrated intensity of 1.3±0.3 K km s^{-1}. The average 3 σ detection limit for the non-detected sources is 0.20 K. In contrast to CO, the CS linewidths of group 1 and 2 sources (if detected) are very similar.

But, as expected from the different CS detection rates (Sect. 4.3.1), the line temperatures and, hence, the integrated intensities differ significantly between the two groups. The mean peak line temperature and integrated intensity for local group 1 sources are 1.1±0.3 K and 1.6±0.4 K km s^{-1} vs. 0.4±0.1 K and 0.7±0.3 K km s^{-1} for group 2, respectively. Considering only the detected (local) group 2 sources, the mean peak line temperature increases to 0.6 K which is still considerably lower than the mean value of the group 1 sources. This shows that dense cores in group 2 globules are not only less frequent than in group 1 globules, but that the cores are, if present, also less dense. The Carina sources have, on average, lower CS peak line temperatures than the local globules which comes probably due to the smaller beam filling factor of the dense gas in these distant objects.

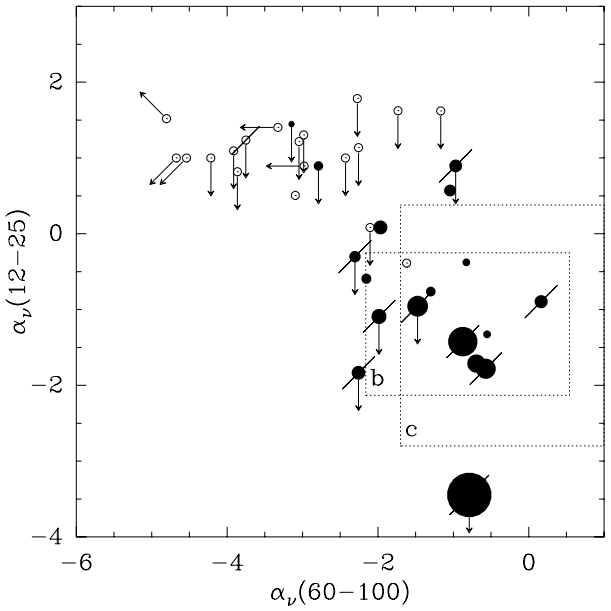

Fig. 8. Colour-colour diagram of all $IRAS$ point sources of our sample. Sources which were detected at 1.3 mm are marked by filled circles. The circle size is scaled with the measured flux density at 1.3 mm. Sources which were not detected at 1.3 mm are marked by open circles. Sources which are associated with molecular outflows are marked by diagonal lines. The arrows give the direction of the shift in the diagram if one considers that some $IRAS$ flux density values are only upper limits. The dotted rectangular boxes mark the same object classes as in Fig. 1.

5. Discussion

5.1. Connection between SEDs, outflows, and dense cores

The presence or absence of dense cores which are a prerequisite for star formation can be tested by the thermal dust emission as well as by molecular line transitions which require high densities to be excited. We found a clear correlation (77%) between the probabilities to detect a source at 1.3 mm continuum and in the CS (2−1) line emission. Out of 35 globules, 17 objects were detected in both tracers (16 of group 1, one of group 2), 10 objects were detected in none of the tracers (3 of group 1, 6 of group 2, one not classified), 7 objects were detected in CS only, and one object was detected at 1.3 mm continuum only.

It was shown in Fig. 6 that there is a clear correlation between the mm continuum flux densities and the CS line peak temperatures of the detected cores. The only (southern) object which deviates considerably from this correlation is DC 267.2−7.2 (group 2, local source). The relatively high CS line temperature (1.5 K) together with the non-detection in the continuum indicate that this globule has a higher density than the other group 2 sources, but a lower column density than the group 1 sources, i.e., it is less centrally condensed than those. This object is a good candidate of a pre-protostellar core being in quasi-static contraction phase prior to collapse (Ward-Thompson et al. 1994).

We found also a clear correlation between the probability to detect a source at 1.3 mm continuum and its position in the $IRAS$ colour-colour diagram (Fig. 8; cf. Sect. 2.1, Fig. 1) which characterizes the spectral slope of the SEDs in two different wavelength ranges . We would like to mention in passing that the SEDs are not only a function of age, but may also depend on the "outer" radiation field and the inclination angle. Nevertheless, it can be clearly seen that the sources of group 1, which have steadily rising SEDs from 12 to 100 μm (see Fig. 2) and FIR colour temperatures of ≈ 25 K, have in general much higher millimetre fluxes than the colder group 2 sources. This looks, at first sight, somewhat surprising since one usually expects the coldest $IRAS$ sources (here group 2) to be the youngest ones and the ones with the most massive dust envelopes. However, as mentioned above, the group 1 sources are "self-embedded" protostars with high column densities (cf. Sects. 4.2.2 and 5.4). The low mm continuum fluxes of the colder group 2 sources indicate that these objects are much less condensed than the group 1 sources and, thus, cannot be representative of the isothermal protostellar phase. Such "isothermal protostars" would appear as compact mm continuum sources (core-envelope) without or with extremely cold and weak FIR counterparts (e.g., VLA 1623; André et al. 1993). Hence, the group 2 sources are either of pre-protostellar nature (cf. Ward-thompson et al. 1994) or they do not form stars at all (cf. discussion in Sect. 5.5).

The results of this survey show that the 1.3 mm dust continuum emission and the CS line emission are equivalent tracers of dense, star-forming molecular cloud cores. The high mm continuum and CS detection rates for the group 1 sources (local globules: 78% in the continuum and 89% in CS) together with the high outflow rate (67%, Sect. 4.3.3) show that these globules harbour dense cores which are in an early stage of star formation. The significantly lower detection rates for the group 2 sources (local globules: 22% in the continuum and 44% in CS) indicate that these globules don't have such dense cores or that their cores are much less dense and compact, respectively.

The far Carina sources ($d > 2$ kpc) are completely excluded from the above discussion. Due to their large distance and, consequently, the large projected beam size, it is very likely that several individual objects contribute to the $IRAS$ fluxes and we see only effective SEDs (cf. Sect. 5.6). The SEDs and the frequency of dense cores of the far Carina sources are, however, not systematically different from those of the local globules.

5.2. Properties of the dense cores

5.2.1. Mass

In order to check the significance of the difference in the detection rates and masses between the two globule goups, we performed a two-sample survival test with the local globules. The test results in a probability of 1±2% for the assumption that both source groups follow the same mass distribution, i.e., the mass distributions are NOT similar at the 5% confidence level. This is demonstrated in Fig. 9 by means of the cumulative Kaplan-Meier estimator of the mass distributions. For the sake of comparison, we perfomed the same test for a subsample of northern globules (Paper I) which was selected with the same

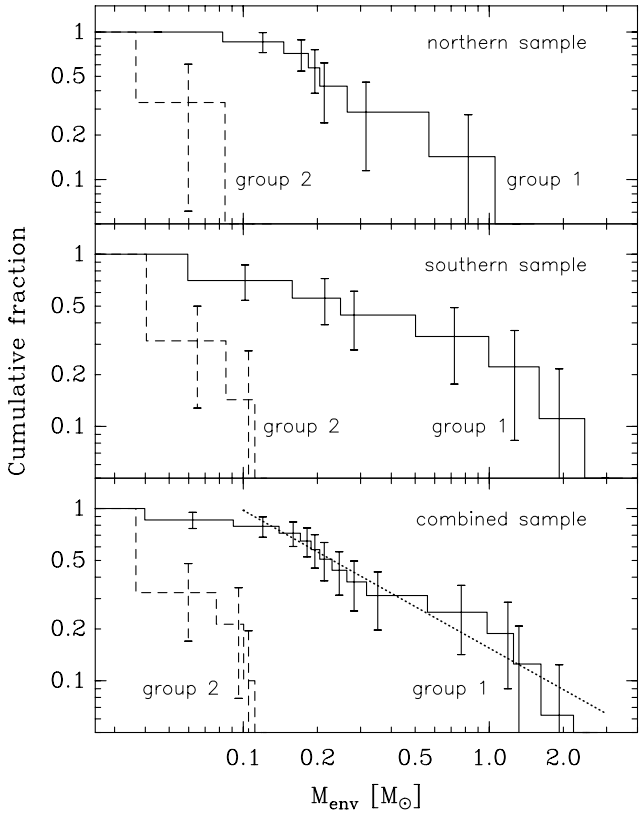

Fig. 9. Cumulative mass distribution of the globule groups 1 (solid lines) and 2 (dashed lines) for the southern (middle panel), northern (upper panel), and combined samples (lower panel). Only globules with $d \leq 500$ pc were taken into account. The masses are derived from the 1.3 mm continuum emission and refer to the beam area only. For group 1 (combined sample) and $M_{\rm env} > 0.15\,{\rm M}_\odot$, the mass spectrum can be fitted by a power law: ${\rm d}N_{\rm cum}/{\rm d}M \propto M^{-0.8}$.

distance restriction. The result is very similar to that of the southern globules, i.e. the mass distributions of group 1 and 2 sources differ significantly from each other and the mass distributions of the northern and southern globule cores (circumstellar envelope masses) are similar at the 75% confidence level. Fig. 9 shows the cumulative mass distributions for the local group 1 and 2 sources in the southern, northern, and combined samples. We use the cumulative form because the differential form does not have a simple analytic error analysis.

The group 1 sources (combined sample) span a wide range of envelope masses from 0.04 to 2.3 $\rm M_\odot$/beam with a mean mass of 0.5±0.15 $\rm M_\odot$. The two most promising Class 0 candidates within our sample (DC 253.3−1.6 and 297.7−2.8; see Sect. 5.4) occupy the upper end of this mass range ($M_{\rm env}$ = 2.3 and 1.3 $\rm M_\odot$). This result corresponds well to the circumstellar envelope masses derived by André & Montmerle (1994) for Class I and 0 sources in the ρ Oph cloud ($M_{\rm env}$ = 0.03 – 2.3 $\rm M_\odot$ $\langle M_{\rm env}\rangle$ = 0.3±0.15 $\rm M_\odot$). The Class 0 candidates in their sample cover again the upper end of this range. In contrast, more than 90% of the group 2 sources have masses below 0.1 $\rm M_\odot$/beam.

The best (logarithmic) fit to the mass distribution of the (local) group 1 sources results in a mass function of the form: ${\rm d}N/{\rm d}M \propto M^{-\alpha}$ with α = 1.8 (differential form). Note, that only 17 data points, of which two are upper limits, were used for this analysis. Although there is some indication that there is a gap in the mass distribution function between 0.3 and 0.7 $\rm M_\odot$ and that the slope is steeper for masses larger than $\approx 0.7\,{\rm M}_\odot$, the total mass range covered can be fitted with a single slope. The number of sources investigated here is too small to discriminate between different power laws (cf. Motte et al. 1998). Note that although the method takes upper limits into account, our sample is sensitivity-limited for masses below 0.15 $\rm M_\odot$/beam. The mass spectrum obtained in this way may be, of course, affected by the fact that the measured fluxes and, thus, the masses, refer to the beam area only and, therefore, depend on the distances. For the upper part of the mass range, we will check the mass distribution with the complete mm continuum maps of 23 globule cores (Launhardt et al. 1998b).

The power law slope of the mass spectrum for circumprotostellar envelopes in Bok globules agrees perfectly with the slope derived for envelope masses of the ρ Oph Class I/0 sources (André & Montmerle 1994). The slope of the envelope mass spectrum agrees also very well with the single-slope clump mass spectrum found in several molecular clouds (α = 1.5. . .1.8; see Kramer et al. 1998 and references therein). The mass spectra obtained by these authors were derived from molecular line maps by Gaussian clump decompositions and span a range in masses of several orders of magnitudes. The similarity in the slopes of the mass distributions of molecular cloud cores and circum-protostellar envelopes in low-mass star-forming regions is remarkable. It suggests that there is a close connection between the fragmentation law in molecular clouds and the stellar initial mass function (IMF). Remember that the IMF for low-mass stars is known to have a slope of $\alpha \approx 1.5$ (e.g., Miller & Scalo 1979). In order to reveal this connection in more detail, a large number of complete maps of well-established protostars with infalling envelopes is required. The fact that the mass spectrum of circum-protostellar envelopes in Bok globules is similar to the envelope mass spectrum as well as to the clump mass spectrum in other dark clouds supports further the assumption that Bok globules are former cloud cores which remain when the thin gas of a molecular cloud dissipates (e.g., by stellar winds or supernova explosions).

5.2.2. Luminosity

The group 1 sources have not only higher masses per beam than the group 2 sources, but also higher bolometric luminosities (6.7±2 $\rm L_\odot$ vs. 1.5±0.4 $\rm L_\odot$, local globules).

A typical, opaque globule receives 1 to 50 $\rm L_\odot$ from the interstellar radiation field (ISRF; e.g., Mathis et al. 1983), depending on the size of the globule and the strength of the radiation field. Since the penetration depth of the radiation field strongly depends on the grain properties, the density profile, and the clumpiness, one can, in general, not discriminate between the contributions from internal and external heating to the total luminosity of the $IRAS$ source without having spatially resolved MIR/FIR maps. In case of the group 1 sources where we see at

shorter wavelengths IR sources smaller than the 100 μm $IRAS$ beam of $2'$, it is clear that a considerable fraction of the total luminosity of the $IRAS$ point source must come from an internal heating source. A quantitative analysis of the luminosity of these sources will be undertaken in Sect. 5.4.

In case of the group 2 sources, this question remains open. The lower luminosities of these sources together with their extremely "cold" SEDs give, however, further evidence that these globules are not yet heated by embedded protostars with their high accretion luminosities (cf. Sect. 5.4). A luminosity of $\approx 1 L_\odot$ is much higher than the expected intrinsic "thermal" luminosity (due to gravitational forces, cf. Ward-Thompson et al. 1994) of such a cloud core, but is consistent with external heating by the ISRF. The average luminosity of the group 2 globule sources ($1.5 \pm 0.4\,L_\odot$) is somewhat higher than the value of $0.9 \pm 0.8\,L_\odot$ derived for a sample of pre-protostellar cores by Ward-Thompson et al. (1994), but agrees within the uncertainty limit. Since the isolated globules are much more exposed to the ISRF than dense cores in larger dark clouds, they must receive more luminosity from the ISRF. This might explain the slightly higher luminosities compared to the pre-protostellar cores studied by Ward-Thompson et al..

5.2.3. Temperature

The kinetic gas temperatures derived from ^{12}CO and NH_3 (9 – 13 K) are much lower than the dust temperatures of the dense cores derived from the broad-band SEDs (≈ 26 K for group 1 and ≈ 20 K for group 2). One reason for this discrepancy may be that gas and dust get in thermal equilibrium only at densities higher than $n_{\rm H} \approx 10^5 - 10^6$ cm^{-3}. The beam-averaged hydrogen densities of the globule cores lie, however, just in this range or are below this value (cf. Sect. 4.2.3). In addition, we already mentioned in Sect. 2.1 that the FIR colour temperature may overestimate the true effective dust temperature of the globule cores.

The more important reason for this discrepancy in gas and colour (dust) temperatures is probably that internally heated cores have a temperature gradient. The relatively "high" colour temperatures and the higher bolometric luminosities of the group 1 sources (together with the presence of molecular outflows) compared to the group 2 sources suggest that these cores are indeed heated by embedded YSOs (cf. discussion in Sect. 5.4). While the optically thin dust continuum emission is dominated by the warm inner region close to the protostar, the optically thick CO line traces only the cooler envelopes in which the gas and dust are de-coupled due to the lower densities. The ammonia observations (Bourke et al. 1995b; Lemme et al. 1996) were performed with relatively large beam sizes and are, therefore, also more sensitive to the cold and extended gas of intermediate density than to the high-density protostellar cores.

No evidence for internal heating was found for the group 2 sources. These objects are probably externally heated (cf. Sects. 5.2.2 and 5.5) and the difference in gas and dust temperatures may be real.

5.3. Outflow energetics

Outflows of low-mass YSOs are closely connected (causal and temporal) to the accretion of mass. Recently, Bontemps et al. (1996) found that the outflow activity declines during the protostellar accretion phase. This means that the youngest protostellar objects being in their main accretion phase ("Class 0" sources) have not only exceptional high $M_{\rm env}/L_{\rm bol}$ ratios (see Sect. 5.4), but lie also an order of magnitude above the well-known correlation between outflow momentum flux and bolometric luminosity observed for embedded YSOs which have passed the main accretion phase (Class I).

Since important outflow parameters such as the flow extent, velocity structure, mass distribution, or inclination angle cannot be derived from one-point measurements of a single line, it is difficult to compare the energetics and evolutionary stages of the outflows. Outflows from low-mass YSOs are generally thought to be momentum-driven (e.g. Masson & Chernin 1993). The effective momentum flux $F = P/T$ (where P is the momentum and T is the time the flow needs to cross the observed region) can, therefore, be assumed to be conserved along the flow direction. Under this assumption, the momentum flux measured within the beam area at the central position should be a characteristic quantity of the outflow which does not depend, at first order, on the projected beam area (distance). Here, we follow the approach of Bontemps et al. (1996) (cf. also Cabrit & Bertout 1992) and compute the momentum flux $F_{\rm CO}$ from:

$$F_{\rm CO} = f(i)\, F_{\rm obs} = f(i)\, M_{\rm wings}\, V_{\rm CO}^2 / R_{\rm CO}$$

where $M_{\rm wings}$ is the total gas mass contained in the wings within the observed area, $V_{\rm CO}$ is the "characteristic" flow velocity, $R_{\rm CO}$ is the radius of the observed area, and $f(i)$ is the inclination correction factor. As the characteristic flow velocity we took the maximum velocity extent from the line center (average of red and blue wing) at the 0.2 K level ($\sim 2\,\sigma$). The HPBW of $23''$ projected at the distance of the object was taken as $2\,R_{\rm CO}$. Both the observed flow velocity and the projected radius along the flow direction depend on the inclination angle i of the outflow ($V_{\rm flow} = V_{\rm rad}/\cos i$, $R_{\rm flow} = R_{\rm proj}/\sin i$). Since we have no information on individual inclination angles, we assume a random distribution of outflow orientations resulting in a mean inclination angle of $\approx 57^\circ$ corresponding to a mean correction factor of $f(i) = 2.9$ (Bontemps et al. 1996).

The largest uncertainty is introduced by the conversion from CO wing emission to the gas mass contained in the outflow wings. It was shown by other authors that the ^{12}CO(2–1) wing emission from outflows in low-mass YSOs is moderately optically thick (e.g. Cabrit & Bertout 1992; Bourke et al. 1997) and that the CO optical depth seems to be constant over the outflow (e.g. Wilking et al. 1990). Therefore, the derivation of the total flow mass from the integrated ^{12}CO(2–1) wing intensity in the optically thin approximation together with an opacity correction gives reasonable results (see Cabrit & Bertout 1990 for a detailed discussion of uncertainties in deriving outflow parameters). For the sake of comparison we adopt the same mean opacity correction factor of 3.5 as Bontemps et al. (1996)

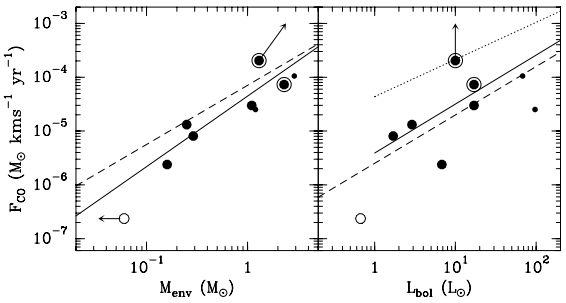

Fig. 10. CO outflow momentum flux $F_{\rm CO}$ vs. circumstellar envelope mass $M_{\rm env}$ and bolometric luminosity $L_{\rm bol}$. The six local ($d < 500$ pc) outflow sources of group 1 are plotted as large filled circles. The symbols of the two Class 0 candidates (DC 253.3−1.6 and 297.7−2.8) are surrounded by larger circles. The two outflow sources (gr. 1) in the near Carina arm are marked by smaller dots. The solid lines represent the "best fit" correlations $F_{\rm CO}$–$M_{\rm env}$ and $F_{\rm CO}$–$L_{\rm bol}$. For comparison, the group 2 source DC 356.5−4.5 (not detected at 1.3 mm continuum) is marked by an open circle. The dashed and dotted lines represent the best fits obtained for other samples of embedded low-mass YSOs by Bontemps et al. (1996) and by Cabrit & Bertout (1992), respectively. Note that these authors used integrated envelope masses derived from maps while we use mass per beam. The arrow marks the shift of DC297.7−2.8 when using the full information from complete mm continuum and CO maps (Bourke et al. 1997).

did in their investigation of outflow activity around low-mass embedded YSOs. This correction factor is consistent with the CO(1–0) optical depth of 2 – 3 measured in the outflow wings of DC 297.7−2.8 by Bourke et al. (1997).

With the method described above we derive momentum fluxes between $2\,10^{-7}$ (DC 297.7−2.8) and $2\,10^{-4}\,{\rm M}_\odot\,{\rm km\,s^{-1}\,yr^{-1}}$ (DC 356.5−4.5), with a mean value of $5.5\,10^{-5}\,{\rm M}_\odot\,{\rm km\,s^{-1}\,yr^{-1}}$ for the local group 1 sources ($d < 500$ pc) and a value of $2\,10^{-7}\,{\rm M}_\odot\,{\rm km\,s^{-1}\,yr^{-1}}$ for the only group 2 source with an outflow detected.

Fig. 10 shows the correlation of the CO momentum flux with the envelope mass (per beam) as derived from the 1.3 mm continuum emission and with the bolometric luminosity of the central IR sources. There is a clear positive correlation ($r = 90\%$) between $F_{\rm CO}$ and the circumstellar envelope mass $M_{\rm env}$. The correlation between $F_{\rm CO}$ and the bolometric luminosity $L_{\rm bol}$ is less clear ($r = 54\%$, only group 1 sources considered), but is still present. The best linear fits for both correlations are:

$$\log\left(\frac{F_{\rm CO}}{{\rm M}_\odot\,{\rm km\,s^{-1}\,yr^{-1}}}\right) = (-4.3\pm0.2) + (1.3\pm0.4)\log\left(\frac{M_{\rm env}}{{\rm M}_\odot}\right) = (-5.4\pm0.6) + (0.9\pm0.7)\log\left(\frac{L_{\rm bol}}{{\rm L}_\odot}\right)$$

The $F_{\rm CO}/M_{\rm env}$ correlation compares well to the results obtained for a sample of 45 embedded YSOs by Bontemps et al. (1996). The $F_{\rm CO}/L_{\rm bol}$ correlation for our sample lies between the correlations derived by Cabrit & Bertout (1991) and by Bontemps et al. (1996). This shows that the link between the outflow energetics and the properties of the protostellar cores cannot be significantly different for Bok globules than for other embedded YSO's in larger molecular clouds. Note, however, that due to the small number of objects in our sample the uncertainty of the fitted correlations is too high to recognize smaller deviations from other source samples.

The high CO momentum flux and envelope mass of DC 297.7−2.8 clearly resembles the properties of the Class 0 sources in the sample of embedded YSOs analysed by Bontemps et al. (1996) (cf. Bourke et al. 1997). The properties of DC 253.3−1.6 and 267.4−7.4 are intermediate to that of Class 0 and Class I sources while the lower CO momentum fluxes of DC267.7−7.4, 275.9+1.9, and 303.8−14.2 give evidence that these objects have passed their main accretion phase. The same holds for the two sources in the near Carina arm (DC 295.0+1.3 and 344.6−4.3). The only group 2 source with a CO line wing (DC 356.5−4.5) has lower values of $F_{\rm CO}$, $M_{\rm env}$, and $L_{\rm bol}$ than the group 1 sources. It is not clear whether this source is distinguished from the group 1 outflow sources only by its lower mass or whether it is already more evolved than those. Another explanation could be that the weak line wing in this source is not caused by an outflow at all (cf. Sect. 4.3.3).

5.4. Evolutionary stage of the group 1 sources

In this paragraph, the evolutionary stage of the local group 1 sources will be discussed together with the mass-luminosity diagram for protostellar systems. The circumstellar masses and the luminosities of the embedded sources will be used in the same way as in Paper I to characterize the evolutionary stage of the (proto-)star-envelope systems (cf. André & Montmerle 1994). Fig. 11 shows the mass-luminosity diagram for our target sources. In the diagram, the observed objects are indicated by their *circumstellar* mass $M_{\rm env}$ and their bolometric luminosity $L_{\rm bol}$, while different theoretical mass-luminosity relations for protostars are indicated by the *stellar* mass M_* and the appropriate luminosity (see below).

The masses of the circumstellar envelopes $M_{\rm env}$ are measured by their optically thin thermal dust emission at mm wavelengths. The masses of the embedded protostars can be derived from the bolometric luminosities $L_{\rm bol}$ under the assumption that the luminosity originates mainly from the accretion shock on the stellar surface. This accretion luminosity (for spherical infall) is given by $L_{\rm acc} = GM_*\dot{M}/R_*(M_*)$, where M_* is the mass of the central star, $\dot{M}$ is the mass accretion rate, and R_* is the stellar radius. Here, we use the mass-radius relation for accreting protostars given by Stahler (1988) and Palla & Stahler (1990). For the mass accretion rate, we use the conservative (low) value of $2\,10^{-6}\,{\rm M}_\odot\,{\rm yr^{-1}}$ (see Paper I). This relation is indicated by the upper dashed line in Fig. 11. The internal luminosity L_* of a star of mass M_* and appropriate radius at the stellar birthline (Fletcher & Stahler 1994) is indicated by the lower dashed line in Fig. 11. During the main accretion phase, L_* is about one order of magnitude smaller than $L_{\rm acc}$. The total luminosity of the protostellar system is then given by the sum of the accretion luminosity $L_{\rm acc}$ and the internal luminosity L_*, as indicated by

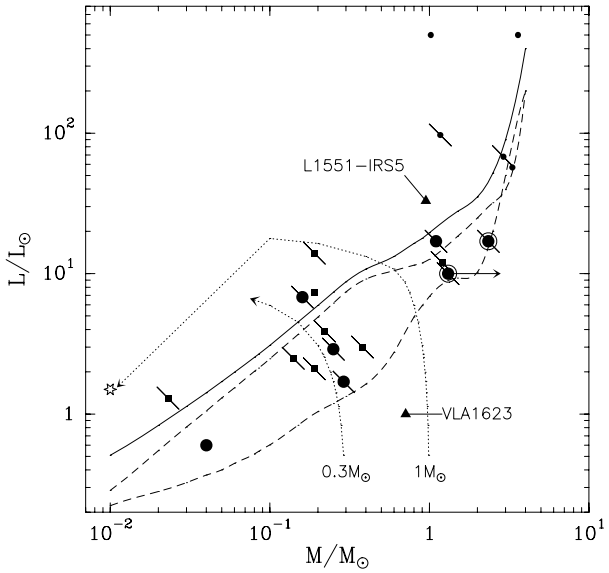

Fig. 11. Mass-luminosity diagram for protostellar cores. The local group 1 sources are plotted as large circles ($L_{\rm bol}$ vs. $M_{\rm env}$ per beam). The symbols of the two Class 0 candidates (DC 253.3−1.6 and 297.7−2.8) are surrounded by larger circles. The arrow to the right indicates the shift of the source DC 297.7−2.8 (BHR 71) in the diagram when using the integrated mass (Bourke et al. 1997). For comparison, the local group 1 sources from the northern globule sample (rectangles, Paper I), the near Carina sources (small circles), as well as VLA 1623 and L1551-IRS5 (triangles, SEST fluxes and bolometric luminosities from Saraceno et al. 1996). For all sources, the same dust opacity and temperature was used to convert the mm fluxes into masses. Outflows are indicated by diagonal lines. The dashed lines mark the theoretical M_*/L relations for accreting protostars ($L_{\rm acc}$, $\dot{M} = 2\,10^{-6}$ M$_\odot$ yr^{-1}, upper curve) and for stars at the stellar birthline (L_*, lower curve, see text). The solid line marks the M_*/L relation when using $L_{\rm bol} = L_{\rm acc} + L_*$. The dotted curves show the evolutionary tracks of the $M_{\rm env}/L_{\rm bol}$ ratio of two protostellar systems of 0.3 and 1 M$_\odot$. The asterisk marks the $M_{\rm env}/L_{\rm bol}$ ratio of a typical T Tauri star. Note that the abscissa stands for the stellar mass (solid and dashed curves) as well as for the circumstellar envelope mass (all other symbols)!

the solid curve in Fig. 11. Due to several uncertainties in the parameters and model assumptions, we consider the lowest (L_* vs. M_*) and uppermost ($L_{\rm acc}$+L_* vs. M_*) curves as boundaries of the uncertainty region of the protostellar mass-luminosity relation.

Under the assumptions that the mass accretion rate and the total mass of the system $M_{\rm tot}$ remain constant during the main accretion phase, the circumstellar (envelope) mass is given by $M_{\rm env} = M_{\rm tot} - t_{\rm c}\,\dot{M}$, where $t_{\rm c}$ is the time since the onset of the collapse (see Paper I for a more detailed discussion of the derivation of these quantities). The expected evolutionary tracks of the $M_{\rm env}/L_{\rm bol}$ ratio of two protostellar systems of 0.3 and 1 M$_\odot$ are shown as dotted lines in Fig. 11 Similar evolutionary tracks were already derived by Saraceno et al. (1996).

An object with $M_{\rm env} > M_*$ must be located on the (lower) right side of the protostellar $M_*/L_{\rm bol}$ relation. Assuming that the entire envelope will be finally accreted onto the star, such objects have accreted less than 50% of their final mass hitherto and are, therefore, still in the main accretion phase. Such "Class 0" protostars (André et al. 1993) usually drive powerful outflows. Objects which have already accreted more than half of the total initial envelope mass and are, thus, more evolved, are located on the upper left side of this $M_*/L_{\rm bol}$ relation (cf. Saraceno et al. 1996). For the sake of comparison, we show the locations of VLA 1623 ("Class 0") and L1551-IRS5 ("Class I") in the diagram.

The average mass-luminosity ratio of the local group 1 sources is $M_{\rm env}/L_{\rm bol} = 0.1\pm0.05$ M$_\odot$/L$_\odot$ (0.08 ± 0.05 M$_\odot$/L$_\odot$ for northern and southern objects). This value is somewhat smaller than the average $M_{\rm env}/L_{\rm bol}$ ratio of 0.3 ± 0.2 derived for 9 Class 0 sources, but larger than the $M_{\rm env}/L_{\rm bol}$ ratio of 0.05 ± 0.05 derived for a large number of Class I sources by Saraceno et al. 1996. For the sake of comparison, we applied the same dust temperature and opacity to their 1.3 mm fluxes as we did to our sources. Three objects in our sample have $M_{\rm env}/L_{\rm bol}$ ratios higher than 0.1 M$_\odot$/L$_\odot$ (DC 253.3−1.6, 297.7−2.8, and 303.8−14.2). These objects lie very close to the lower boundary of the protostellar $M_*/L_{\rm bol}$ relation and have, thus, very likely $M_{\rm env} > M_*$. All three sources drive molecular outflows and the first two of them have the most powerful outflows within our sample (see Sect. 4.3.3). These objects are the most promising candidates within our sample for being "Class 0" protostars.

The objects DC 267.4−7.5, 275.9+1.9, and 320.5−3.6 lie in the transition region between $M_{\rm env} > M_*$ and $M_{\rm env} < M_*$. These objects are presumably very young, but no statement can be made here about their exact evolutionary stage. DC 267.7−7.4 is the outflow candidate with the lowest circumstellar mass ($M_{\rm env} = 0.16$ M$_\odot$) and it is associated with a visible star at the $IRAS$ position. It is also the most evolved source in the sense that it has the lowest $M_{\rm env}/L_{\rm bol}$ ratio (0.024). The near Carina objects resemble rather the properties of Class I than of Class 0 sources, although their larger distance (and projected beam size) does not allow a reliable interpretation.

The least massive one of the local group 1 sorces detected at 1.3 mm continuum is DC 320.5−3.6. In contrast to all other group 1 sources detected at 1.3 mm, no outflow was found in this source. It is not clear whether this object drives no or an extremely weak outflow due to its low mass or whether it is in an earlier (pre-protostellar) stage than the other group 1 sources.

Note that the circumstellar masses were derived from On-On measurements and refer to the beam area only. They are, therefore, lower limits of the total circumstellar masses. In contrast to this, the $IRAS$ fluxes and, thus, the IR luminosities originate from the entire dense cores due to the large beam of $IRAS$. Therefore, the $M_{\rm env}/L_{\rm bol}$ ratios derived here are lower limits. For DC 297.7–2.8, a typical very young protostellar core (group 1, "Class 0"), the shift in the diagram when using the integrated circumstellar mass is shown by an arrow (data from Bourke et al. 1997).

Although the exact position of the objects in the $M_{\rm env}/L_{\rm bol}$ diagram and their evolutionary stage can only be derived from maps of the continuum emission and from complete SEDs, the diagram shows that the the globule cores of group 1 are

in an early stage of star formation and reveal the properties of "Class 0" and "Class I" protostars. The youngest ones of these objects are still in their main accretion phase and must, therefore, have core masses which are of the same order as the masses of the stars which they will finally form. The average envelope mass of all local group 1 sources is $0.5\pm0.15\,M_\odot$, while the average mass of the three Class 0 candidates (see above) is $1.3\pm0.8\,M_\odot$. We conclude, therefore, that Bok globules form stars with typical masses of the order of $1\,M_\odot$.

5.5. The nature of group 2 sources

In Paper I we speculated that the group 2 sources are mostly pre-protostellar cores and that the less opaque ones could probably be cirrus clouds since they match the FIR colours of cirrus clouds. There are, however, two arguments against the cirrus hypothesis:
1. In most diffuse cirrus clouds ^{12}CO cannot be seen due to photodissociation (e.g., Blitz et al. 1990). However, in all group 2 sources observed so far, ^{12}CO was detected and was, on average, not considerably weaker than in the group 1 sources.
2. Cirrus clouds usually have a visual extinction of $A_V < 1$ mag (e.g., Stark 1995). However, using the method described by Wood et al. (1994) together with the most conservative dust temperature estimate of $T_d = 25$ K, we derive visual extinctions of $A_V = 4.6...11.4$ mag ($\langle A_V\rangle = (6.8\pm2.2)$ mag) for the group 2 sources of this sample from the 100 μm source fluxes. Using a more realistic dust temperature of $T_d = 20$ K, the average A_V increases to 13 mag. This is consistent with group 2 sources in the northern sample (Paper 1) where we derive $\langle A_V\rangle = 10$ mag from ^{12}CO (CYH91) and $\langle A_V\rangle = 12$ mag from the *IRAS* data ($T_d = 20$ K).

Hence, the group 2 globules are rather "real" dark clouds with cores just compact and dense enough to be detected by *IRAS*, probably only due to their isolated location. Comparable objects in larger dark clouds would not have enough contrast to the surrounding cloud to be detected by *IRAS* as point sources.

In Sect. 5.2.2 we pointed out that the bolometric luminosities of these objects could be completely due to external heating by the ISRF, so that no statement can be made about the contribution of a possible internal heating source, except that it must have a lower luminosity than the total luminosity ($\langle L\rangle = 1.5\,L_\odot$). Although the beam-averaged densities of these sources (Sect. 4.2.3) are about five times lower than the values derived by Ward-Thompson et al. (1994) for a sample of pre-protostellar cores in dark clouds, we speculate that those group 2 globule cores which were detected in the CS line (DC 268.2−9.7, 267.2−7.2, and 319.9−4.8), or in the mm continuum (DC 249.4−5.1), or in both tracers (DC 289.3−2.8) are in a pre-protostellar stage. However, complete maps of the mm continuum and CS line emission are required to reveal the true nature of these sources.

The other group 2 sources which were not detected in the CS line nor in the mm continuum may have some kind of dense core (100 μm *IRAS* point source!). But, their cores are probably not massive and dense enough to form stars. Another explanation could be that they already formed very low-mass stars (or even brown dwarfs) which did not completely destroy the core. The group 2 is, thus, much less homogeneous than the group 1 and no easy classification criterion seems to exist which can be used to distinguish between the different alternative explanations.

5.6. The nature of the Carina sources

The sources in the near Carina arm ($0.7 \le d \le 1.3$ kpc) are not significantly different than the local globules. The CO and CS linewidths as well as the CO line temperatures (and, hence, the kinetic gas temperatures) are comparable to that of the local globules. Due to the selection effect, their avearge size and mass are somewhat larger than those of the local globules. Their bolometric luminosities are by about one order of magnitude higher than those of the local globules, which is also a selection effect. As a result, the objects in the near Carina arm are, on average, more evolved than the local group 1 globules in the sense that they have lower envelope mass to bolometric luminosity ratios. However, they still resemble the typical properties of globules with embedded low-mass YSOs of mainly "Class I".

The sources in the far Carina arm ($2.2 \le d \le 4.4$ kpc) are not typical of "classical" globules. While the typical size of a globule is ≈ 0.5 pc, these clouds have sizes of 5 to 10 pc which is larger than, e.g., the ρ Oph cloud core. These clouds are, very likely, more complex structured than globules and they have probably more than one star-forming core. Such clouds would not have been identified as Bok globules if they were located at shorter distances. According to their masses and luminosities, they are, however, also low-mass (or intermediate-mass) star-forming regions and do not form high-mass stars. When putting the ρ Oph cloud at a distance of 3 kpc, its central part would appear like a diffuse globule, and its star-forming cores, which harbour rhich clusters of YSOs (e.g., L 1689, Wilking & Lada 1983), would appear as unresolved IR sources in the *IRAS* beam with a total luminosity of the order of $1000\,L_\odot$. Therefore, we propose that the sources in the far Carina arm are cores of dark cloud complexes with embedded clusters of low-mass YSOs. The higher kinetic gas temperature compared to the local globules (cf. Sect. 4.3.2) also suggests the presence of additional heating sources like, e.g., embedded clusters of YSOs. High-resolution imaging of the infrared sources and of the mm dust continuum and molecular line emission (e.g., ^{13}CO and CS) is required to reveal the true nature of these objects.

6. Summary and conclusions

In search for dense, star-forming cores and molecular outflows we surveyed 35 southern Bok globules for 1.3 mm dust continuum emission as well as ^{12}CO (2–1) and CS (2–1) line emission. This is the first comprehensive survey of Bok globules in the southern sky using these tracers. There is an overlap of 20 globules with the ammonia survey of Bourke et al. (1995b) which makes these two surveys a valuable database for further, more detailed investigations of individual globules. The globules were selected from the catalogues of Hartley et al. (1986)

and Feitzinger & Stüwe (1984). The selection criteria were: (1) isolated location and compact and opaque appearance and (2) association with a cold $IRAS$ point source ($T_{\rm FIR} < 35$ K). The second criterion clearly biased our sample towards globules with young star-forming cores, in accordance with the goal of this study.

Five globules (marked in Table 4.2) were studied in more detail. The results for DC 297.7−2.8 were already published (Bourke et al. 1997). The results for the other four globules will be published in a succeeding paper.

The main results and conclusions can be summarized as follows:

1. For the first time, reliable it distance estimates were obtained for most of the globules of our sample. A very efficient method of associating the globules with larger molecular cloud complexes was used. Although Bok globules seem to appear as isolated objects, they are, in most cases, still loosely connected with the molecular cloud complexes from which they were originally formed. Half of the objects is located in the local spiral arm at distances between 100 and 400 pc (average distance 300 pc). The most prominent features in the spatial distribution of these globules are the Lindblad ring and the Vela-Gum complex. Eight globules are located at the near side of the Carina arm at distances between 0.7 and 1.3 kpc, and 6 objects are in the far Carina arm at distances beyond 2 kpc. The latter 6 objects are larger and more massive than "normal" globules.
2. Out of the 35 globules observed, all globules were detected in the ^{12}CO(2–1) line (detection rate 100% at a 3 σ detection limit of $T_{\rm mb} = 0.3$ K), 24 globules were detected in the CS(2–1) line (detection rate 69% at a 3 σ detection limit of $T_{\rm mb} = 0.2$ K), and 18 globules were detected in the 1.3 mm continuum emission (detection rate 51% at a 3 σ detection limit of 40 mJy/beam). In 12 globules (34%), CO line wings indicating the presence of molecular outflows have been found, of which 8 outflows were previously unkown. The colours of the embedded $IRAS$ point sources, the mm dust continuum emission, the CS (and NH_3) line emission as well as the presence of molecular outflows are all well correlated with each other. We found that the 1.3 mm dust continuum emission and the CS line emission are equivalent tracers for the detection of dense, star-forming molecular cloud cores. Therefore, reliable statements on the nature and evolutionary stage of the individual objects could be made.
3. The objects could be divided into it two groups according to the location in the $IRAS$ colour-colour diagram. Group 1 turned out to represent self-embedded protostars (star-forming globule cores with embedded Class 0 and Class I objects). Group 2 comprises non- and pre-star-forming globule cores. In comparison to Paper I, no "star-less" cores nor group 3 objects are contained in this southern sample.
4. The *group 1* globule cores span a range in masses between 0.15 $M_\odot$ (sensitivity limit) and 2.3 $M_\odot$ with a mean mass of 0.6±0.25 $M_\odot$ and a slope of the mass distribution $\mathrm{d}N/\mathrm{d}M$ of −1.8. The beam-averaged column and number densities of these cores are $\langle N_{\rm H}\rangle = (5\pm5)\,10^{22}{\rm cm}^{-2}$ and $\langle n_{\rm H}\rangle = (8\pm5)\,10^{5}{\rm cm}^{-3}$, respectively. The mean CO and CS linewidths (Gaussian HPWs) are 2.3±0.25 K and 1.3±0.2 K, respectively. Two thirds of the group 1 globules have *molecular outflows*, which ultimatively proofs that these globules form new stars. The momentum fluxes of these outflows compare well to the values derived for Class 0 and I sources in dark cloud complexes.
5. The *group 2* globule cores are less massive, more diffuse, and more quiescent than the group 1 sources. Their SEDs are steeply rising from 60 to 100 μm and they were mostly not detected at shorter wavelengths. These globules usually don't have outflows. Their beam-averaged column and number densities are $\langle N_{\rm H}\rangle = (1\pm0.5)\,10^{22}$ cm^{-2} and $\langle n_{\rm H}\rangle = (6\pm3)\,10^{4}$ cm^{-3} (mostly upper limits), respectively. The mean CO and CS linewidths (Gaussian HPWs) are 1.6±0.1 K and 1.3±0.2 K, respectively. We checked that these objects are not simply cirrus clouds, but rather belong to the group of dark clouds.
6. The *youngest sources* within our sample which clearly resemble the properties of Class 0 protostars being in their main accretion phase are DC 297.7−2.8 and 253.3−1.6. These objects have envelope masses of the order of 2 $M_\odot$, $M_{\rm env}/L_{\rm bol}$ ratios of 0.13 $M_\odot/L_{\rm bol}$, and drive the most powerful outflows. The sources in DC 267.4−7.5 and 303.8−14.2 have properties intermediate between Class 0 and Class I objects. The globules DC 267.7−7.4 and 275.9+1.9 harbour more evolved YSOs of Class I. The other local group 1 sources and the objects in the near Carina arm resemble the properties of Class I YSOs, although no clear statement can be made about their exact evolutionary stage.
7. Candidates for *pre-protostellar cores* within our sample are DC 249.4−5.1, 267.2−7.2, 268.2−9.7, 289.3−2.8, and 319.9−4.8. These group 2 objects are associated with extremely cold $IRAS$ sources. They do not show well-condensed cores in the CS line nor in the 1.3 mm continuum emission. The other group 2 sources don't have cores which are compact and massive enough to form solar-like stars.
8. The objects in the *far Carina arm* ($d > 2$ kpc) are assumed to be cores of dark cloud complexes with embedded clusters of low-mass YSOs.
9. The (beam-averaged) kinetic gas *temperatures* are in the range between 10 and 15 K, while the broad-band SEDs are consistent with (mass-averaged) dust temparatures of the order of 25 to 30 K for group 1 sources and of 20 K for group 2 sources. This discrepancy can be partially explained by internal heating, optical depth effects, and thermal decoupling of gas and dust in the envelopes.
10. We could clearly confirm our finding from Paper I that Bok globules form solar-like stars with typical masses between 0.5 and 1 $M_\odot$. More massive dark clouds resembling the simple structure of globules are rare. In contrast to the globules, such clouds often contain multiple cores and are able to form clusters of low-mass stars.

Acknowledgements. We would like to thank the referee for critical comments which helped to improve the clarity of the paper. RL was supported by the Verbundforschung Astronomie/Astrophysik contract No. 50 OR 9414 9.

References

André P., Ward-Thompson D., Barsony M., 1993, ApJ 406, 122
André P., Montmerle T., 1994, ApJ 420, 837
Blitz L., Bazell D., Désert F.X., 1990, ApJ 352, L13
Bontemps S., André P., Terebey S., Cabrit S., 1996, A&A 311, 858
Bourke T.L., Hyland A.R., Robinson G., 1995a, MNRAS 276, 1025 (BHR)
Bourke T.L., Hyland A.R., Robinson G., James S.D., Wright C.M., 1995b, MNRAS 276, 1067
Bourke T.L., Garay G., Lehtinen K.K., et al., 1997, ApJ 476, 781
Brand J., Blitz L., Wouterloot J.G.A., 1986, A&AS 65, 537 (BBW)
Brand J., Wouterloot J.G.A., 1988, A&AS 75, 177
Brand J., Blitz L., 1993, A&A 275, 67
Brandt J.C., 1971, in: Maran S.P., Brandt J.C., Stecher T.P (eds.), The Gum Nebula and Related Problems, NASA SP-322, 4
Cabrit S., André P., 1991, ApJ 379, L25
Cabrit S., Bertout C., 1992, A&A 261, 274
Chernin L.M., Masson C.R., 1991, ApJ 382, L93
Chernin L.M., Masson C.R., 1995, ApJ 455, 182
Clemens D.P., Barvainis R., 1988, ApJS 68, 257 (C&B88)
Clemens D.P., Sanders D.B., Scoville N.Z., 1988, ApJ 327, 139
Clemens D.P., Yun J.L., Heyer M., 1991, ApJS 75, 877 (CYH91)
Dame T.M., Ungerechts H., Cohen R.S., et al., 1987, ApJ 322, 706
Dopita M.A., Schwartz R.D., Evans I., 1982, ApJ 263, L75
Emerson J.P., 1987, IRAS and star formation in dark clouds. In: Peimbert M., Jugaku, K.J. (eds.) Star Forming Regions. Reidel, Dordrecht, p.19
Fletcher A.B., Stahler S.W., 1994, ApJ 435, 313
Feigelson E.D., Nelson P.I., 1985, ApJ 293, 192
Feitzinger J.V., Stüwe J.A., 1984, A&AS 58, 365
Gordon M. A., 1995, A&A 301, 853
Grabelsky D.A., Cohen R.S., Bronfman L., Thaddeus P., 1987, ApJ 315, 122
Hartley M., Manchester R.N., Smith R.M., Tritton S.B., Goss W.M., 1986, A&AS 63, 27
Hawarden T.G., Brand P.W.J.L., 1976, MNRAS 175, 19P
Henning Th., Michel B., Stognienko R., 1995, Planet. Space Sci. 43, 1333
Hodapp K.-W., Ladd E.F., 1995, ApJ 453, 715
Kramer C., Stutzki J., Röhrig R., Corneliussen U., 1998, A&A 329, 249
Kreysa, E., 1990, Sub-mm direct photometry with large telescopes. In: ESA, From Ground-Based to Space-Borne Sub-mm Astronomy. p.265
Kutner M.L., Ulich B.L., 1981, ApJ 250, 341
Lada C., 1987, Star formation - From OB associations to protostars. In: Peimbert M., Jugaku, K.J. (eds.) Star Forming Regions. Reidel, Dordrecht, p.1
Launhardt R., Mezger P.G., Haslam C.G.T., et al., 1996, A&A 312, 569
Launhardt R., Henning Th., 1997, A&A 326, 329 (Paper I)
Launhardt R., Ward-Thompson D., Henning Th., 1997, MNRAS 288, L45
Launhardt R., Evans II N.J., Wang Y., et al., 1998a, ApJS 119, in press
Launhardt R., Henning Th., Zylka R., 1998b, in preparation
LaValley M., Isobe T., Feigelson E.D., 1992, "ASURV", Bull. Am. Astron. Soc.
Lehtinen K., 1997, A&A 317, L5
Lemme C., Wilson T.L., Tieftrunk A.R., Henkel C., 1996, A&A 312, 585
Lindblad P.O., Grape K., Sandquist A., Schober J., 1973, A&A 24, 309
Lynds B.T., 1962, ApJS 7, 1
Masson C.R., Chernin L.M., 1993, ApJ 414, 230
Mathis J.S., Mezger P.G., Panagia N., 1983, A&A 128, 212
Men'shchikov A.B., Henning Th., 1997, A&A 318, 879
Meurs E.J. A., Harmon R.T., 1988, A&A 206, 53
Morgan J.A., Bally J., 1991, ApJ 372, 505
Motte F., André P., Neri R., 1998, A&A , in press
Neckel T., Klahre G., 1980, A&AS 42, 251
Neckel T., Chini R., Güsten R., Wink J.E., 1985, A&A 153, 253
Olberg M., Reipurth B., Booth R., 1992, A&A 259, 252
Ossenkopf V., Henning Th., 1994, A&A 291, 943
Palla F., Stahler S.W., 1990, ApJ 360, L47
Penzias A.A., Burrus C.A., 1973, ARA&A 11, 51
Persi P., Ferrari-Toniolo M., Busso M., et al., 1990, AJ 99, 303
Persi P., Ferrari-Toniolo M., Marenzi A.R., et al., 1994, A&A 282, 233
Reipurth B., 1983, A&A 117, 183
Reipurth B., Chini R., Krügel E., Kreysa E., Sievers A., 1993, A&A , 273, 221
Sandqvist Aa., 1977, A&A 57, 476
Sandqvist Aa., Lindroos K.P., 1976, A&A 53, 179
Saraceno P., André P., Ceccarelli C., Griffin M., Molinari S., 1996, A&A 309, 827
Schwartz R.D., 1977, ApJ 212, L25
Seidensticker K.J., Schmidt-Kaler Th., 1989, A&A 225, 192
Stahler S.W., 1988, ApJ 332, 804
Stark R., 1995, A&A 301, 873
Terebey S., Chandler C.J., André P., 1993, ApJ 414, 759
Ward-Thompson, D., Scott, P.F., Hills, R.E., André, P., 1994, MNRAS 268, 276
Westin T.N.G., 1985, A&A 60, 99
Wilking B.A., Lada C.J., 1983, ApJ 274, 698
Wilking B.A., Lada C.J., Young E.T., 1989, ApJ 340, 823
Wilking B.A., Blackwell J.H., Mundy L.G., 1990, AJ 100, 758
Whittet D.C.B., Assendorp R., Prusti T., Roth M., Wesselius P.R., 1991, A&A 251, 524
Wood D.O.S., Myers P.C., Daugherty D.A., 1994, ApJS 95, 457
Wouterloot J.G.A., Henkel C., Walmsley C.M., 1989, A&A 215, 131
Yun J.L., Clemens D.P., 1992, ApJ 385, L21
Zealey W.J., Ninkov Z., Rice E., Hartley E., Tritton S.B., 1983, Astrophys. Lett., 23, 119
Zhou S., Evans II N.J., Kömpe C., Walmsley C.M., 1993, ApJ 404, 232